

NACA RM L50D14

12 JUL 1950

UNCLASSIFIED

# NACA

## RESEARCH MEMORANDUM

LOW-SPEED LATERAL STABILITY AND AILERON-EFFECTIVENESS  
CHARACTERISTICS AT A REYNOLDS NUMBER OF  $3.5 \times 10^6$   
OF A WING WITH LEADING-EDGE SWEEPBACK DECREASING  
FROM  $45^\circ$  AT THE ROOT TO  $20^\circ$  AT THE TIP

By Roy H. Lange and Huel C. McLemore

Langley Aeronautical Laboratory  
Langley Air Force Base, Va.

CLASSIFIED DOCUMENT

This document contains classified information affecting the National Defense of the United States within the meaning of the Espionage Act, USC 5031 and 5042. The transmission or the revelation of its contents in any manner to an unauthorized person is prohibited by law. Information so classified may be imparted only to persons in the military and naval services of the United States, appropriate civilian officers and employees of the Federal Government who have a legitimate interest therein, and to United States citizens of known loyalty and discretion who of necessity must be informed thereof.

NACA LIBRARY  
LANGLEY AERONAUTICAL LABORATORY  
Langley Field, Va.

### NATIONAL ADVISORY COMMITTEE FOR AERONAUTICS

WASHINGTON

July 6, 1950

CLASSIFICATION CANCELLED

Authority J. W. Crowley 12/11/53  
EO 10501  
By [Signature] 11/16/54  
See NACA  
L.S.V. Fy

## NATIONAL ADVISORY COMMITTEE FOR AERONAUTICS

## RESEARCH MEMORANDUM

## LOW-SPEED LATERAL STABILITY AND AILERON-EFFECTIVENESS

CHARACTERISTICS AT A REYNOLDS NUMBER OF  $3.5 \times 10^6$ 

OF A WING WITH LEADING-EDGE SWEEPBACK DECREASING

FROM  $45^\circ$  AT THE ROOT TO  $20^\circ$  AT THE TIP

By Roy H. Lange and Huel C. McLemore

## SUMMARY

Results are presented of an investigation of the lateral stability and aileron-effectiveness characteristics of a wing with the leading-edge sweepback decreasing from  $45^\circ$  at the root to  $20^\circ$  at the tip. The wing has an aspect ratio of 4.12 and NACA 64A009 airfoil sections and is equipped with a plain unsealed 18.3-percent-chord aileron. The investigation was made for the basic wing and for the wing with split flaps, leading-edge flaps, outboard slats, and combinations of these high-lift devices at a Reynolds number of about  $3.5 \times 10^6$ .

The effective-dihedral parameter is positive up to stall for all configurations investigated with a maximum value of 0.0033 being measured for the wing with split flaps deflected  $60^\circ$ . All the configurations investigated are directionally stable throughout the lift-coefficient range. The value of the aileron-effectiveness parameter for all the configurations investigated is about 0.0010 at 85 percent of maximum lift coefficient and the aileron investigated can provide lateral trim up to about  $12^\circ$  yaw. In general, the lateral-stability and aileron-effectiveness results obtained for the subject wing are comparable to those obtained for essentially unswept wings.

## INTRODUCTION

A general investigation has been conducted in the Langley full-scale tunnel on a wing plan form designed to diminish the inherent tip-stalling tendencies of sweptback wings. The leading-edge sweepback of the wing decreases in three steps from  $45^\circ$  at the root to  $30^\circ$  at the midsemispan and to  $20^\circ$  at the tip. The wing has an aspect ratio of 4.12,

a taper ratio of 0.36, and NACA 64A009 airfoil sections. The maximum-lift and longitudinal characteristics of the wing at Reynolds numbers from  $2.4 \times 10^6$  to  $6.0 \times 10^6$  are reported in reference 1, and the chord-wise and spanwise pressure distributions are given in reference 2. The results of references 1 and 2 indicated that the wing plan form under consideration had characteristics comparable to those obtained for conventional sweptback wings of moderate sweepback. As a part of the general low-speed investigation, tests have been made to determine the lateral stability and aileron-effectiveness characteristics of the basic wing and of the wing with high-lift devices installed.

The data presented herein for the lateral-stability investigation consist of force measurements for angles of attack through stall of the basic wing and of the wing with split flaps and full-span leading-edge flaps installed for angles of yaw from about  $-5^\circ$  to  $16^\circ$ . Data are also presented from tests made to determine the effectiveness of a plain unsealed 18.3-percent-chord aileron on the basic wing and on the wing with split flaps, leading-edge flaps, outboard slats, and combinations of these high-lift devices for angles of attack through stall at zero yaw. All the data are presented for a Reynolds number of about  $3.5 \times 10^6$  and a Mach number of about 0.07.

#### COEFFICIENTS AND SYMBOLS

The test data are presented as standard NACA coefficients of forces and moments referred to the standard stability axes as indicated in figure 1. The origin of the system of axes is located in the plane of symmetry as projected from the quarter chord of the mean aerodynamic chord.

$C_L$	lift coefficient (Lift/qS)
$C_{L_{max}}$	maximum lift coefficient
$C_X$	longitudinal-force coefficient (X/qS)
$C_Y$	lateral-force coefficient (Y/qS)
$C_m$	pitching-moment coefficient ( $M/qS\bar{c}$ )
$C_n$	yawing-moment coefficient ( $N/qSb$ )
$C_l$	rolling-moment coefficient ( $L/qSb$ )
pb/2V	wing-tip helix angle, radians

$C_{lp}$	damping-in-roll coefficient; rate of change of rolling-moment coefficient with wing-tip helix angle $\left(\frac{\partial C_l}{\partial \frac{pb}{2V}}\right)$
Lift = -Z	
Z	vertical force
X	longitudinal force
Y	lateral force
M	pitching moment about Y-axis
N	yawing moment about Z-axis
L	rolling moment about X-axis
$\rho$	mass density of air
V	free-stream velocity
$\Lambda$	angle of sweepback at leading edge, degrees
A	aspect ratio ( $b^2/S$ )
q	free-stream dynamic pressure ( $\rho V^2/2$ )
S	wing area
$\bar{c}$	mean aerodynamic chord measured parallel to plane of symmetry (7.28 ft) $\left(\frac{2}{S} \int_0^{b/2} c^2 dy\right)$
b	span of wing
$\lambda$	taper ratio
p	angular velocity about X-axis
c	local chord
y	spanwise coordinate
$\alpha$	angle of attack measured in plane of symmetry, degrees

$\psi$	angle of yaw (positive when right wing is rearward), degrees
$C_{L\alpha}$	rate of change of lift coefficient with angle of attack, per degree
$C_{Y\psi}$	rate of change of lateral-force coefficient with angle of yaw, per degree
$C_{N\psi}$	rate of change of yawing-moment coefficient with angle of yaw, per degree
$C_{L\psi}$	rate of change of rolling-moment coefficient with angle of yaw, per degree
$C_{L\delta}$	rate of change of rolling-moment coefficient with aileron deflection, per degree
$\delta_a$	aileron deflection, degrees
$\delta_f$	split-flap deflection, degrees
$\delta_{at}$	total (equal up and down) aileron deflection, degrees

#### MODEL

The geometric characteristics of the wing and the arrangement of the high-lift devices are given as figures 2 and 3. Photographs of the model mounted for tests in the Langley full-scale tunnel are given as figure 4. The airfoil section is the NACA 64A009 parallel to the plane of symmetry. The wing-tip shape is one-half of a body of revolution of the airfoil section. The wing has no geometric dihedral or twist. Further description of the wing construction and the high-lift devices is given in reference 1.

The wing is equipped with a plain unsealed 18.3-percent-chord aileron located on the outer 35 percent of the right wing panel. (See fig. 5.) The aileron deflections are remotely controlled by an actuator within the wing.

#### TESTS

In order to determine the lateral stability characteristics of the wing, force tests were made in yaw for the basic wing and for the wing with split flaps deflected  $60^\circ$ , full-span leading-edge flap, and a

combination of the split and full-span leading-edge flaps. These configurations were investigated for angles of yaw from about  $-5^{\circ}$  to  $16^{\circ}$  and for angles of attack from about  $0^{\circ}$  through stall. The tests in yaw were made with the aileron gaps sealed and faired.

Aileron-effectiveness tests were made for the basic wing and for the wing with the full-span leading-edge flap, 35-percent-span leading-edge slats, 35-percent-span leading-edge flaps, and combinations of these configurations with the split flaps deflected  $60^{\circ}$ . These configurations were tested at several pertinent angles of attack which were determined from inspection of the lift curves and tuft studies of reference 1. The aileron was located on the right wing panel only and was deflected through a range of  $\pm 24^{\circ}$ .

All the tests were made at a Reynolds number of about  $3.5 \times 10^6$  (based on the mean aerodynamic chord) and a Mach number of about 0.07.

## RESULTS AND DISCUSSION

### Presentation of Results

The results have been corrected for the stream misalignment, blocking effects, and jet-boundary effects. No tests were made to determine the support tare and interference effects, inasmuch as all the investigations of wings made recently on the same wing supports have shown these effects to be negligible.

The results of the tests are grouped into two main sections. The first section presents the lateral stability characteristics of the wing as determined from tests in yaw. This section includes figures 6 to 8. The second section presents the results of the aileron-effectiveness tests and includes figures 9 to 19. The summary curves of the aileron characteristics given in figures 9 to 11 include the aileron effectiveness in figure 9, the rolling and yawing moments for total aileron deflection in figure 10, and the rolling effectiveness for the basic wing in figure 11. The basic data from the aileron-effectiveness tests for several wing-flap configurations are presented in figures 12 to 19.

### Static Lateral Stability Characteristics

The lateral-stability parameters  $C_{l_{\psi}}$ ,  $C_{n_{\psi}}$ , and  $C_{y_{\psi}}$  for the basic wing and for the wing with high-lift devices installed are presented as a function of lift coefficient in figure 6. These parameters were determined at zero yaw from the variations of  $C_l$ ,  $C_n$ , and  $C_y$  with  $\psi$  given in the typical data plots of figures 7 and 8.

Dihedral effect.- Positive dihedral effect is measured up to stall for all configurations investigated. (See fig. 6.) The maximum value of  $C_{l_{\psi}}$  for the basic wing of 0.0014 is increased to 0.0021 with the full-span leading-edge flap installed alone, and to 0.0033 with the split flaps installed alone. The addition of the full-span leading-edge flaps to the latter configuration reduces the maximum value of  $C_{l_{\psi}}$  to about 0.0026.

Since the angle of sweepback at the leading edge of the subject wing varies from root to tip, it is difficult to determine a basis for a comparison of the results of the present tests with those obtained for conventional sweptback wings. The following table of  $C_{l_{\psi}}$  values is given, therefore, for the basic wing and wing with split flaps deflected (where flap span is comparable) as a means of evaluating the lateral characteristics of the wing.

$(C_{l_{\psi}})_{max}$		$\Lambda$ (deg)	$\lambda$	A	Airfoil section	Wing
$\delta_f = 0^\circ$	$\delta_f = 60^\circ$					
0.0033	0.0043	34	0.44	4.84	<sup>1</sup> NACA 0015 root NACA 23009 tip	Reference 3
.0038	-----	30	1.00	4.36	<sup>1</sup> NACA 23012	Reference 4
.0012	-.0001	5	.55	4.62	<sup>1</sup> NACA 0015 root NACA 23009 tip	Reference 3
.0018	-----	0	1.00	4.13	NACA 23012	Reference 4
.0014	.0033	45 to 20	.36	4.12	NACA 64A009	Subject Wing

<sup>1</sup>Airfoil sections not parallel to plane of symmetry.

From the foregoing data it appears that the maximum dihedral effect of the subject wing is comparable to that obtained for essentially unswept wings.

Directional stability and lateral force.- As shown by the curves of  $C_{n_{\psi}}$  given in figure 6, all the configurations investigated are directionally stable throughout the lift-coefficient range, and the static directional stability increases with increasing lift coefficient up to stall.

The value of  $C_{n\psi}$  at stall increases from -0.0006 for the basic wing to a maximum value of about -0.0017 for the wing with the combination of split and full-span leading-edge flaps installed.

The values of the lateral-force parameter  $C_{Y\psi}$  are only slightly affected with increasing lift coefficient for all configurations investigated (fig. 6), and the effect of the split flaps is to decrease the value of  $C_{Y\psi}$ .

#### Aileron Characteristics

Aileron effectiveness.- The aileron-effectiveness parameter  $C_{l\delta}$  for the basic wing and for the wing with the high-lift devices installed is presented in figure 9. The values of  $C_{l\delta}$  determined at  $\delta_a = 0^\circ$  are derived from the basic data of figures 12 to 19. Lift coefficients corresponding to  $0.85C_{L_{max}}$  which are considered representative of those usable for the landing condition are noted in figure 9 for purposes of comparison.

For the configurations without the split flaps installed, the values of  $C_{l\delta}$  at  $0.85C_{L_{max}}$  are 0.0011 for the basic wing, 0.00105 for the wing with full-span leading-edge flap installed, and about 0.0010 for the wing with the slat and  $0.35b/2$  leading-edge flaps installed. These values of  $C_{l\delta}$  were not appreciably changed by the addition of split flaps. After the occurrence of leading-edge separation at the wing tips at angles of attack of  $12.8^\circ$  and  $9.3^\circ$  (references 1 and 2) for the basic wing and wing with split flaps, respectively, there is a rapid loss in aileron effectiveness with increasing angle of attack such that at the angles of attack for maximum lift the value of  $C_{l\delta}$  is about one-half of that measured at  $0.85C_{L_{max}}$ . (See fig. 9.) The addition of the slat or the leading-edge flap to the outer 35 percent of the span prevents the large loss in effectiveness at the higher angles of attack by eliminating the flow separation in the region of the tips (reference 1). A further improvement in the aileron effectiveness at the higher angles of attack is obtained with the full-span leading-edge flap installed where there is no loss in effectiveness for angles of attack up to maximum lift ( $\alpha = 19.4^\circ$ ). In addition, this configuration is the only one for which the aileron effectiveness is maintained past stall. The addition of split flaps to the latter configuration results in only a small loss in effectiveness at maximum lift ( $\alpha = 17.7^\circ$ ). The addition of the split flaps to the wing with the slat or leading-edge flap in the outer 35 percent of the span, however, results in a rapid loss in

effectiveness at the higher angles of attack which is attributed to an increase in the severity of the flow breakdown observed at the inboard end of the slat or flap (reference 1). There is no appreciable difference in the aileron effectiveness throughout the angle-of-attack range of the wing with either the slat or  $0.35b/2$  leading-edge flap installed.

Using the methods of reference 5, calculations of the aileron-effectiveness parameter  $C_{l\delta}$  (at  $\alpha = 0^\circ$ ) were made for several conventional sweptback wings which had the same aspect ratio and taper ratio as the subject wing but differed in the amount of leading-edge sweepback. The results of these calculations indicate that the value of  $C_{l\delta}$  calculated for a wing with  $10^\circ$  leading-edge sweepback was about the same as that measured for the subject wing.

Rolling- and yawing-moment characteristics.- The rolling-moment coefficient obtained with a total aileron deflection of  $48^\circ$  in the low angle-of-attack range (below  $\alpha = 10^\circ$ ) is about 0.040 for all configurations investigated. (See fig. 10(a).) For the higher angles of attack the split flaps cause a large decrease in  $C_l$ , except for the full-span leading-edge-flap configuration. The rolling-moment curves for the full-span leading-edge-flap configuration are discontinuous between angles of attack of about  $18.4^\circ$  and  $20^\circ$  (fig. 10(a)) and between aileron deflections of  $-8^\circ$  to  $-12^\circ$  (fig. 14(a)). Inasmuch as the data of reference 1 revealed that the full-span leading-edge-flap configuration was susceptible to sudden stalling of either wing tip for angles of attack near that for maximum lift, the discontinuities are attributed to stalling of the right wing tip as indicated by the lift curves of figure 14(b). The data of figures 7(a), 8(a), and 10(a) indicate that sufficient aileron control (based on aileron data at zero yaw) is available to trim out the rolling moments associated with about  $12^\circ$  of yaw for all configurations except for the split-flap configuration at the higher angles of attack where aileron control is available up to about  $8^\circ$  of yaw. The aileron in most instances is still effective at the maximum deflection tested of  $24^\circ$  and could probably attain a greater deflection and some additional trim in yaw.

Adverse yawing-moment coefficients are obtained throughout the angle-of-attack range for all configurations tested, the largest values of which are obtained for the wing with leading-edge high-lift devices installed. (See fig. 10(b).)

Rolling effectiveness.- In order to indicate a measure of the rolling effectiveness of the aileron investigated, values of the wing-tip helix angle  $\text{pb}/2V$  have been calculated for two conventional wings of  $0^\circ$  and  $30^\circ$  sweepback which had the same aspect ratio and taper ratio as the

subject wing. The range of sweepback is considered sufficient to represent the characteristics of the plan form under consideration. The estimated values of  $\frac{pb}{2V}$  were determined in the usual manner from the relationship  $\frac{pb}{2V} = \frac{C_L}{C_{L_p}}$ . The values of  $C_{L_p}$  were determined from the expression

$$C_{L_p} = (C_{L_p})_{C_L=0} \frac{(C_{L_\alpha})_{C_L}}{(C_{L_\alpha})_{C_L=0}}$$

given as method 1 in reference 6. The values of  $(C_{L_p})_{C_L=0}$  for an aspect ratio of 4.12 and a taper ratio of 0.36 obtained from the charts of reference 6 were -0.3175 for  $0^\circ$  sweepback and -0.3050 for  $30^\circ$  sweepback. The values of  $\frac{pb}{2V}$  presented have not been corrected for the effects of adverse yaw or wing twist, and an aileron linkage system giving a differential of 1:1 (equal up and down deflections) is assumed.

The data of figure 11 show that the total aileron deflection required to produce a helix angle of  $0.09$  considered necessary for satisfactory low-speed control as specified in reference 7 decreases from about  $29^\circ$  at an angle of attack of  $3.5^\circ$  to about  $22^\circ$  at an angle of attack of  $12.8^\circ$ . The data also show a small effect of sweepback for the range of sweepback and angles of attack considered.

Pitching-moment characteristics.- The curves of pitching-moment coefficient against lift coefficient given in figures 12 to 19 show, in general, a very small increment in pitching-moment coefficient resulting from  $24^\circ$  up and down deflection of the aileron for lift coefficients up to  $0.85C_{L_{max}}$ .

#### SUMMARY OF RESULTS

The results of an investigation of the low-speed lateral stability and aileron-effectiveness characteristics of a wing with the leading-edge sweepback decreasing from  $45^\circ$  at the root to  $20^\circ$  at the tip are summarized as follows:

1. Positive dihedral effect is measured up to stall for all configurations investigated. The maximum value of  $C_{L_\psi}$  is increased from 0.0014 for the basic wing to 0.0033 for the wing with split flaps deflected  $60^\circ$ . The addition of the full-span leading-edge flap to the latter configuration gives a value of 0.0026.

2. All the configurations investigated are directionally stable throughout the lift-coefficient range.

3. The value of the aileron-effectiveness parameter for all configurations investigated is about 0.0010 at  $0.85C_{l_{max}}$ . For angles of attack near maximum lift the addition of split flaps causes an appreciable reduction in the aileron effectiveness for all the configurations except for that with the full-span leading-edge flap installed. The full-span leading-edge-flap configurations maintain the highest values of  $C_{l_{\delta}}$  at the higher angles of attack.

4. For the maximum deflection of  $48^{\circ}$  sufficient aileron control is available for lateral trim up to  $12^{\circ}$  yaw except for the split-flap configuration which can trim to  $8^{\circ}$  yaw.

5. The lateral-stability and aileron-effectiveness results obtained for the subject wing are comparable with those obtained for essentially unswept wings.

Langley Aeronautical Laboratory  
National Advisory Committee for Aeronautics  
Langley Air Force Base, Va.

## REFERENCES

1. Lange, Roy H.: Maximum-Lift Characteristics of a Wing with the Leading-Edge Sweepback Decreasing from  $45^\circ$  at the Root to  $20^\circ$  at the Tip at Reynolds Numbers from  $2.4 \times 10^6$  to  $6.0 \times 10^6$ . NACA RM L50A04a, 1950.
2. Barnett, U. Reed, Jr., and Lange, Roy H.: Low-Speed Pressure-Distribution Measurements at a Reynolds Number of  $3.5 \times 10^6$  on a Wing with Leading-Edge Sweepback Decreasing from  $45^\circ$  at the Root to  $20^\circ$  at the Tip. NACA RM L50A23a, 1950.
3. McCormack, Gerald M., and Stevens, Victor I., Jr.: An Investigation of the Low-Speed Stability and Control Characteristics of Swept-Forward and Swept-Back Wings in the Ames 40- by 80-Foot Wind Tunnel. NACA RM A6K15, 1947.
4. Letko, William, and Goodman, Alex: Preliminary Wind-Tunnel Investigation at Low Speed of Stability and Control Characteristics of Swept-Back Wings. NACA TN 1046, 1946.
5. Lowry, John G., and Schneider, Leslie E.: Estimation of Effectiveness of Flap-Type Controls on Sweptback Wings. NACA TN 1674, 1948.
6. Goodman, Alex, and Adair, Glenn H.: Estimation of the Damping in Roll of Wings through the Normal Flight Range of Lift Coefficient. NACA TN 1924, 1949.
7. Anon.: Flying Qualities of Piloted Airplanes. U. S. Air Force Specification No. 1815-B, June 1, 1948.

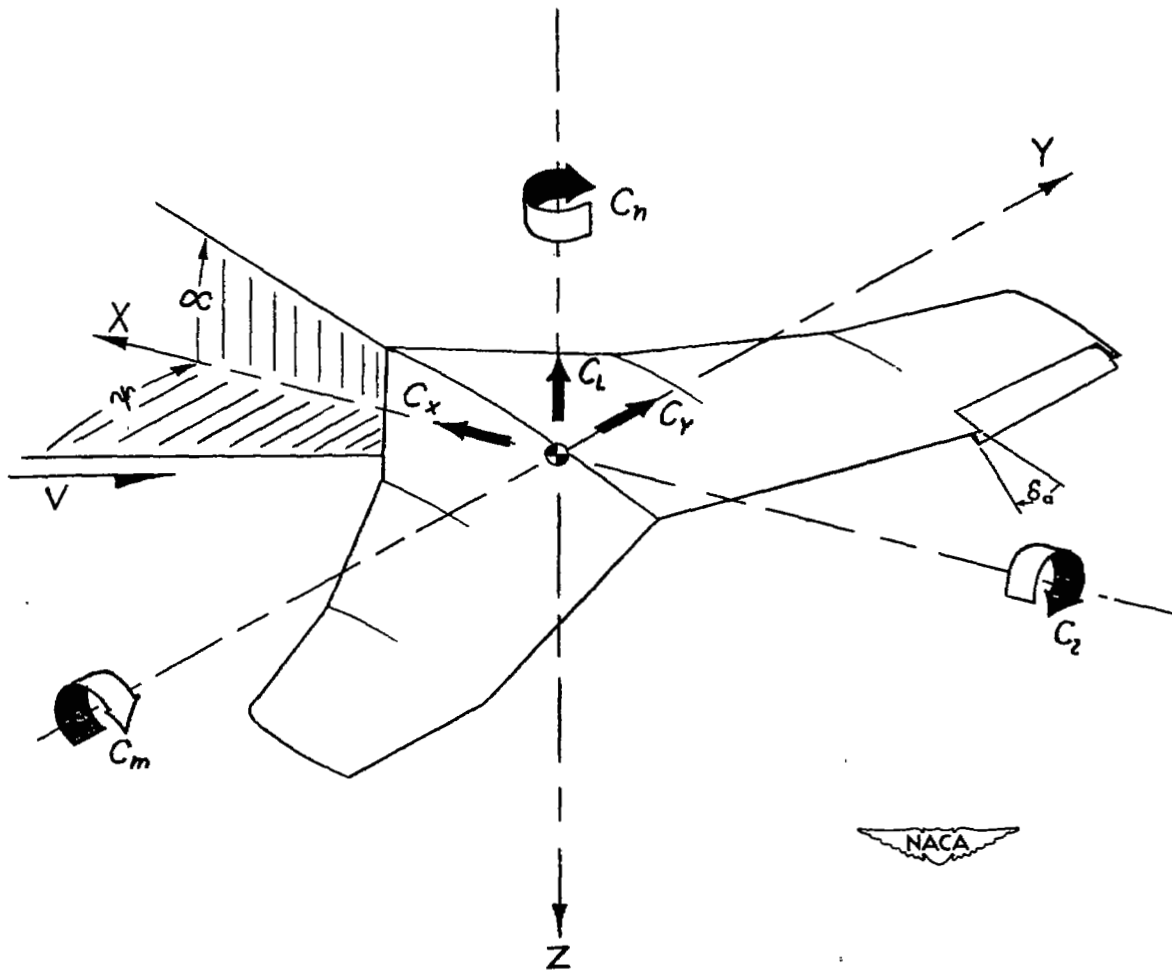
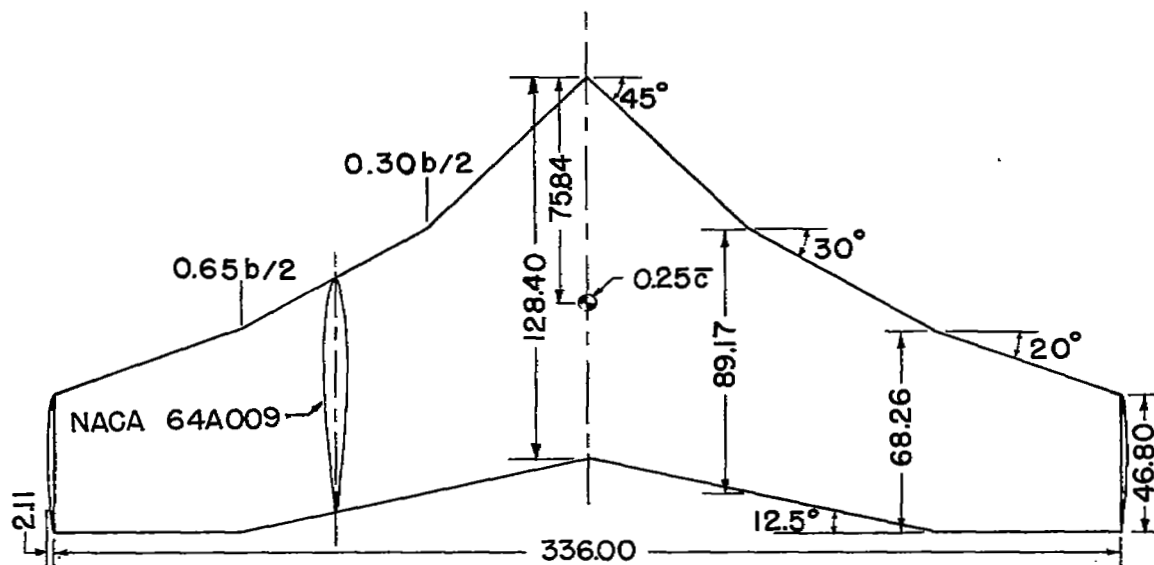


Figure 1.- The stability system of axes and sign convention for the standard NACA coefficients. All forces, force coefficients, moment coefficients, angles, and the control-surface deflection are shown as positive.



Aspect ratio	4.12
Taper ratio	0.36
Wing area	190.24 sq ft

Figure 2.- Geometric characteristics of wing. All dimensions are given in inches.

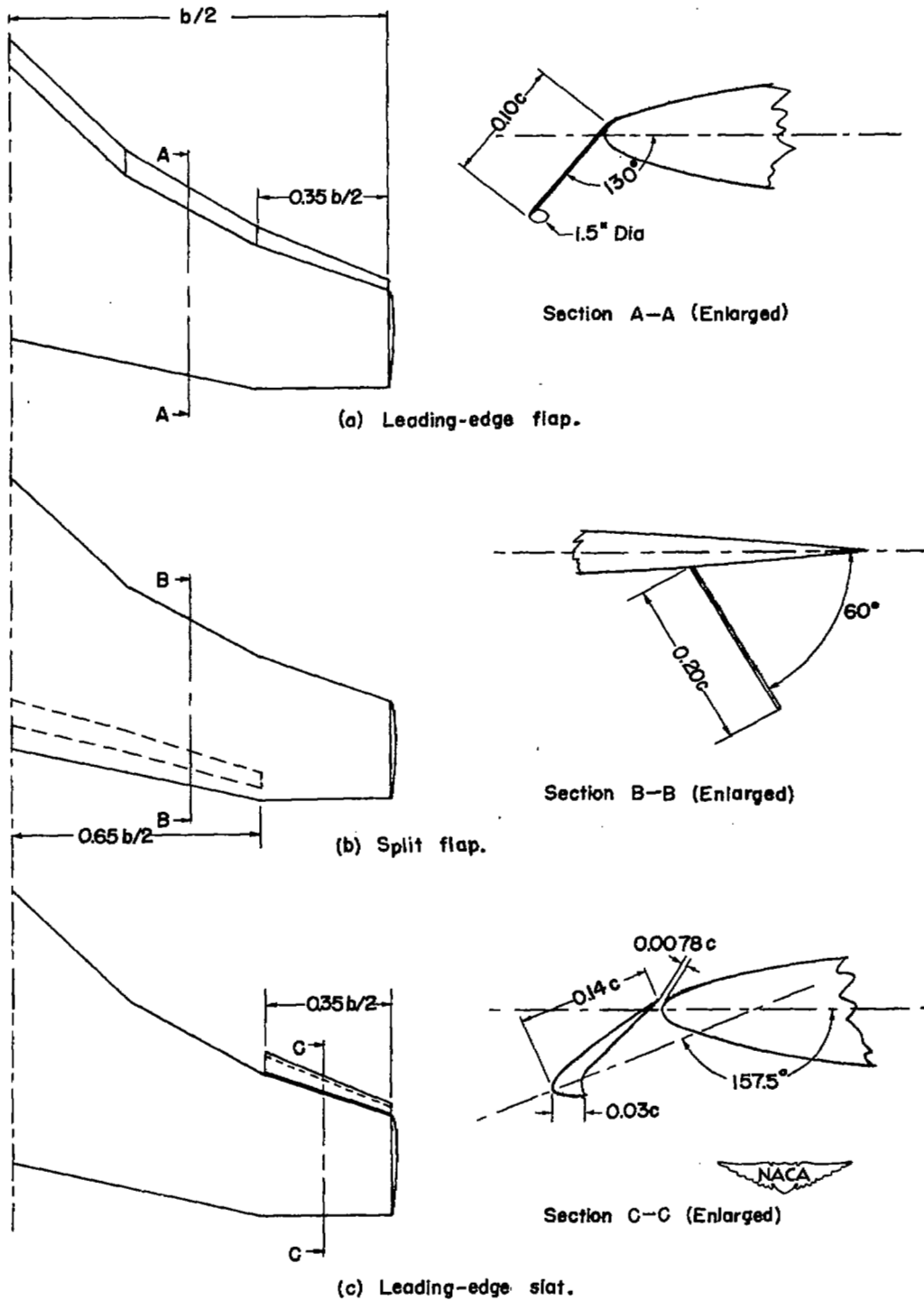
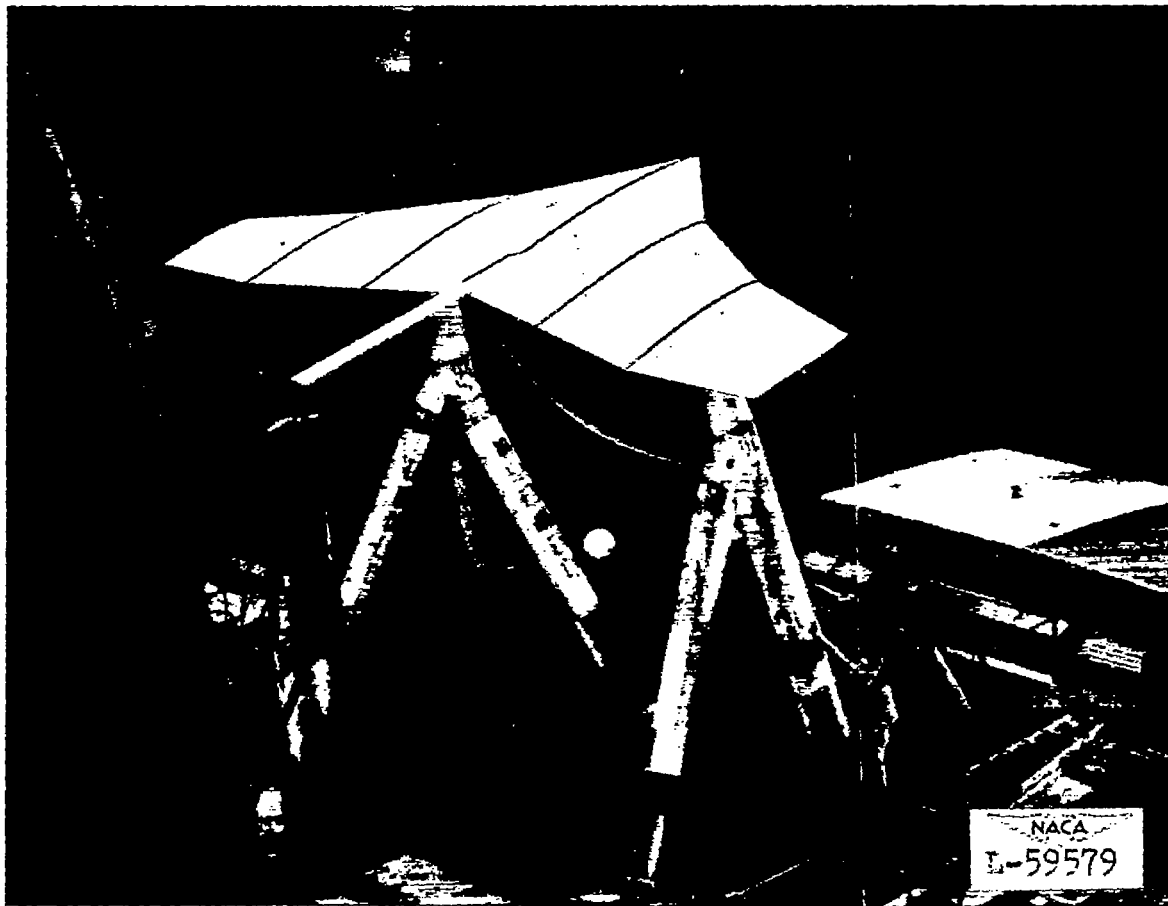


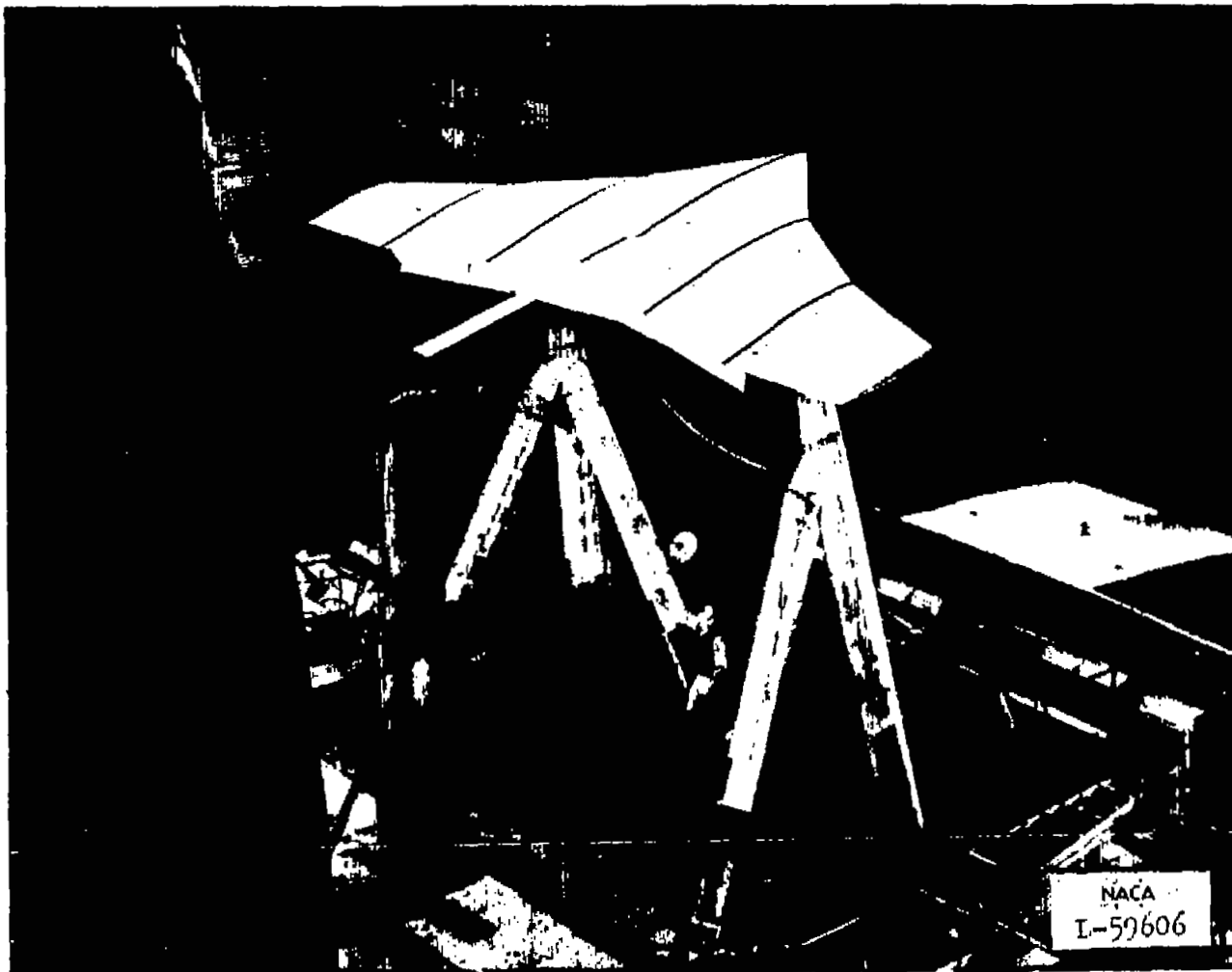
Figure 3.- Arrangement of high-lift devices investigated.



(a) Basic wing.

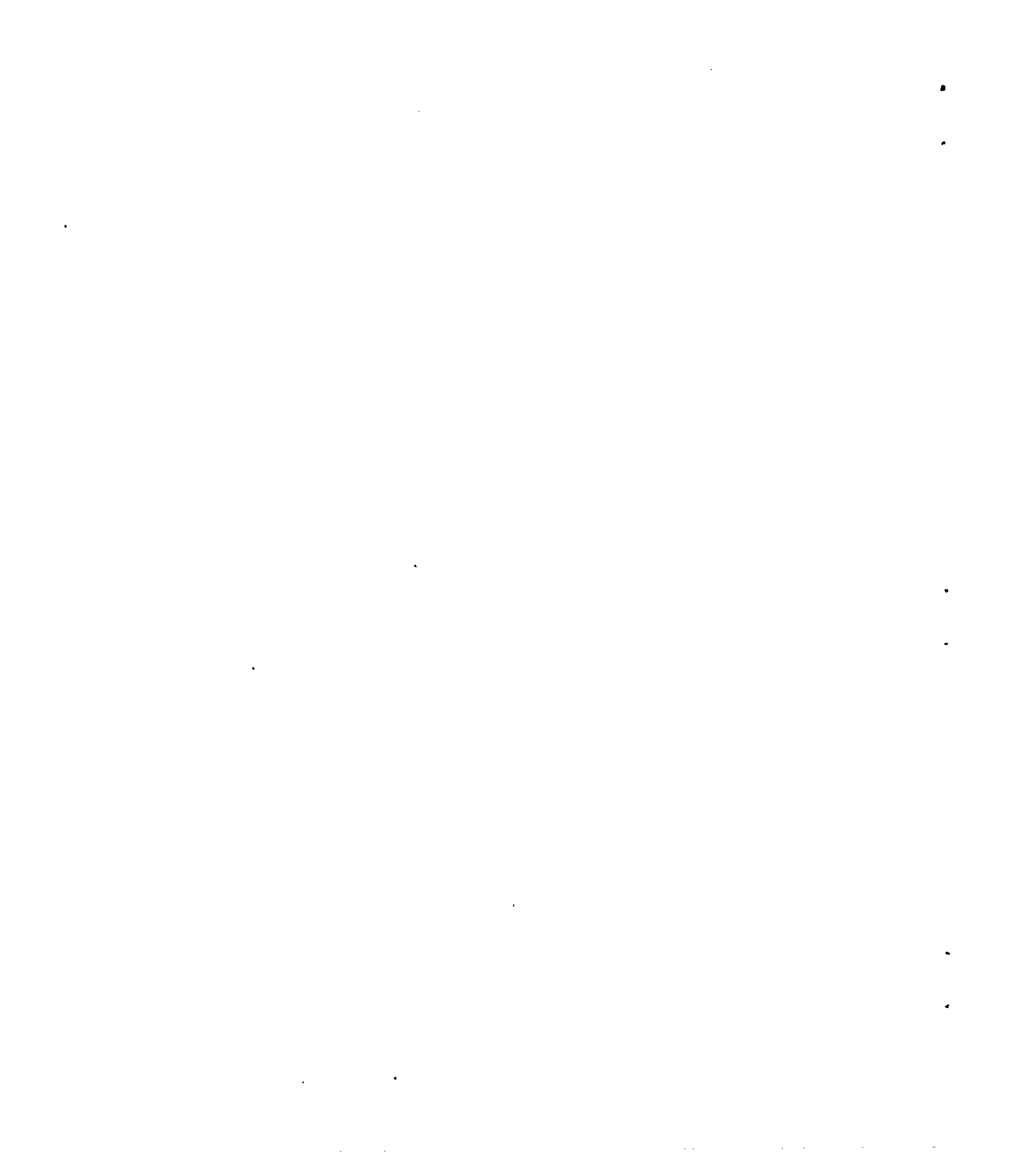
Figure 4.- Photographs of wing mounted in the Langley full-scale tunnel.





(b) Split flaps installed.  $\delta_f = 60^\circ$ .

Figure 4.- Concluded.



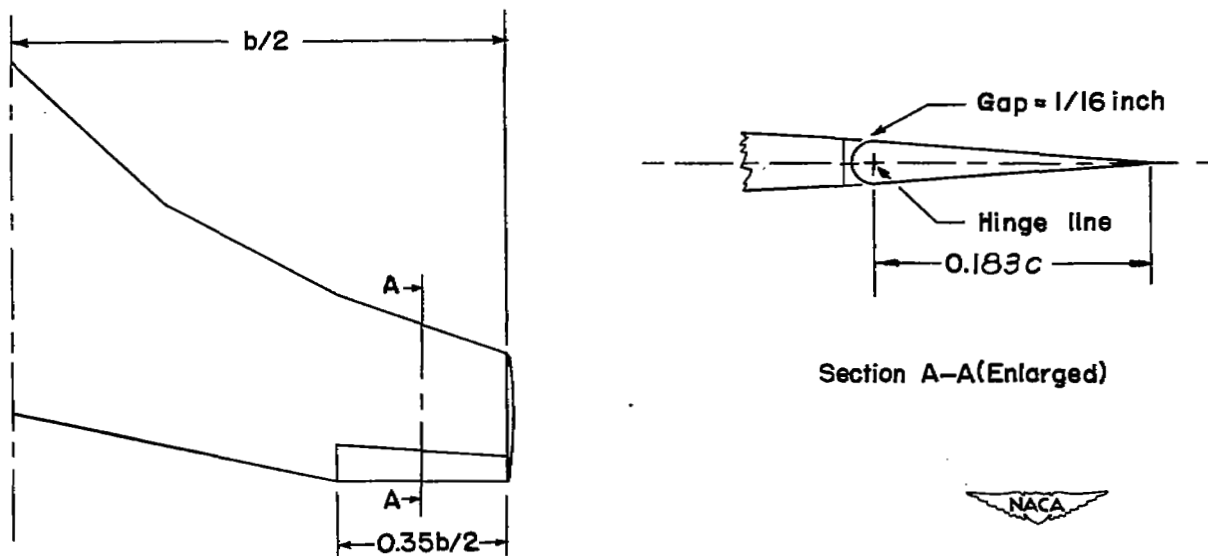


Figure 5.- Geometric characteristics of the plain unsealed aileron.

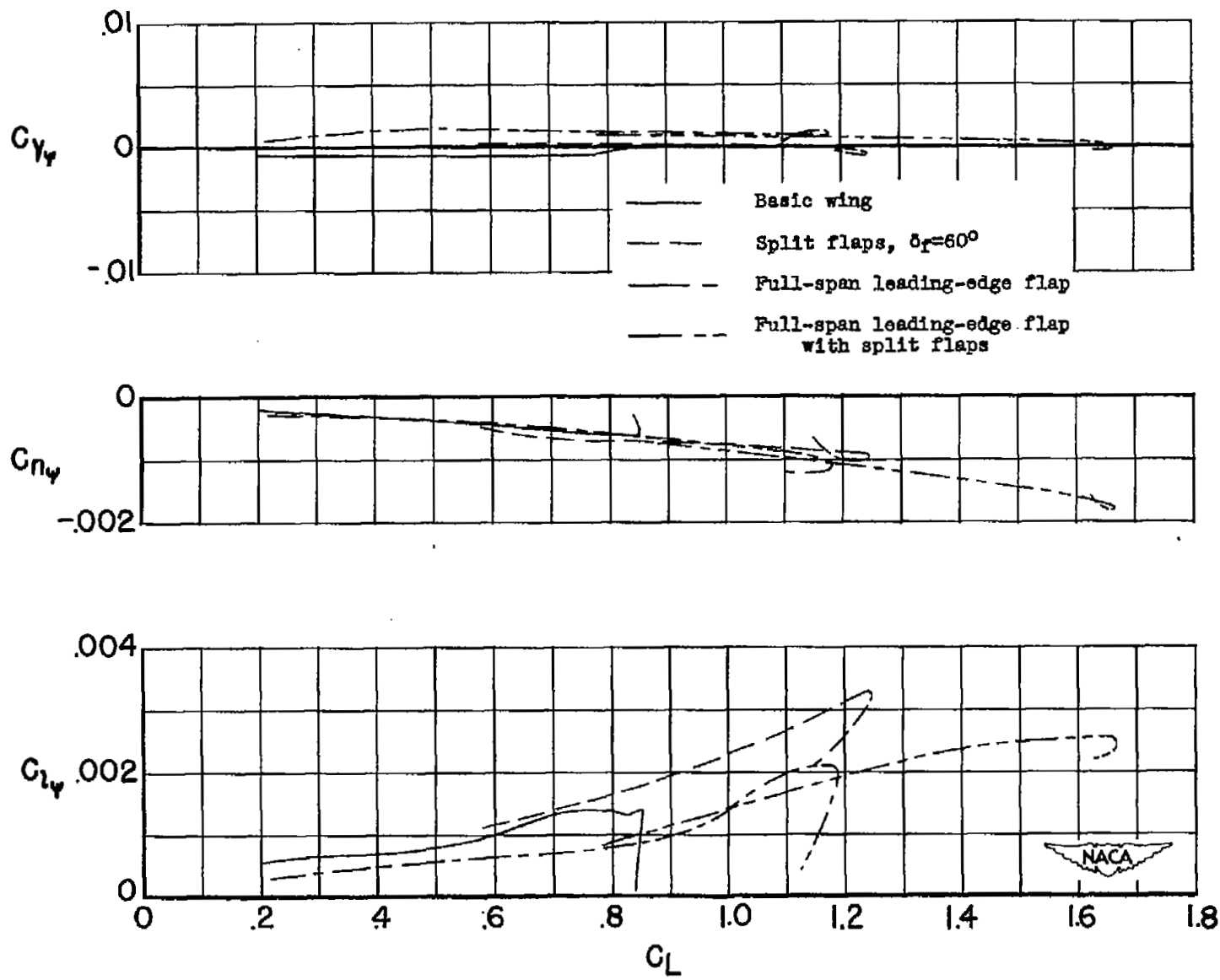
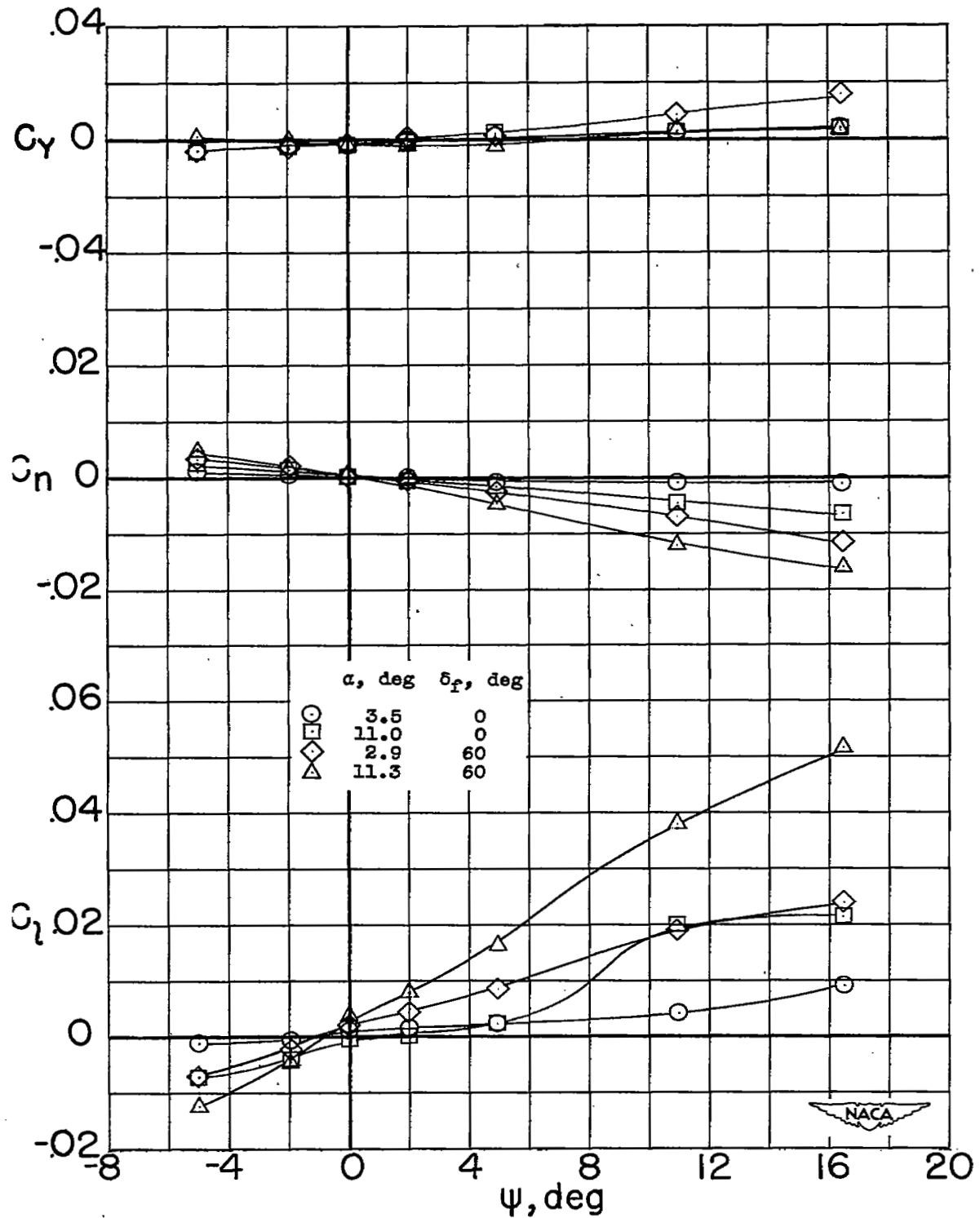


Figure 6.- Summary curves showing the variation of lateral-stability parameters with lift coefficient for several configurations.

$$R \approx 3.5 \times 10^6.$$



(a) Variation of  $C_l$ ,  $C_n$ , and  $C_y$  with  $\psi$ .

Figure 7.- Aerodynamic characteristics in yaw of basic wing and wing with split flaps deflected.  $R \approx 3.5 \times 10^6$ .

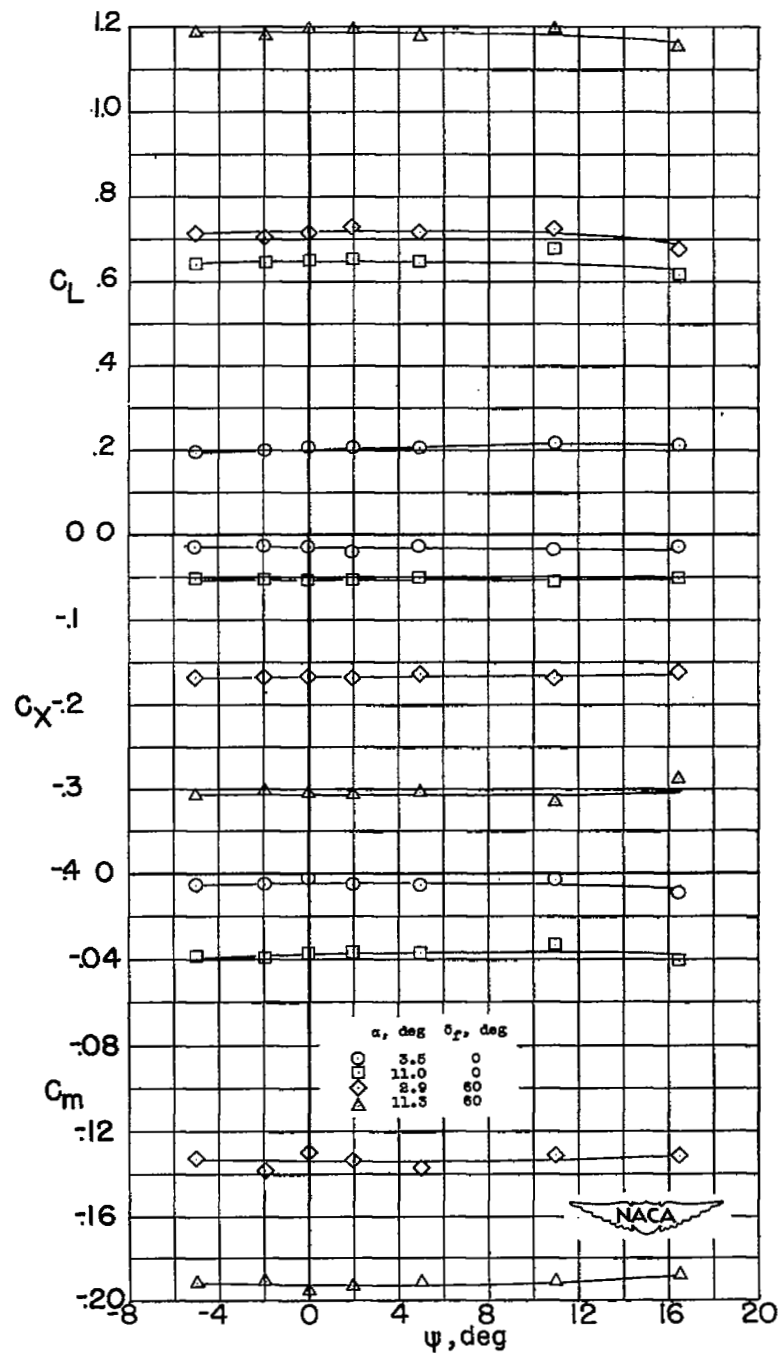
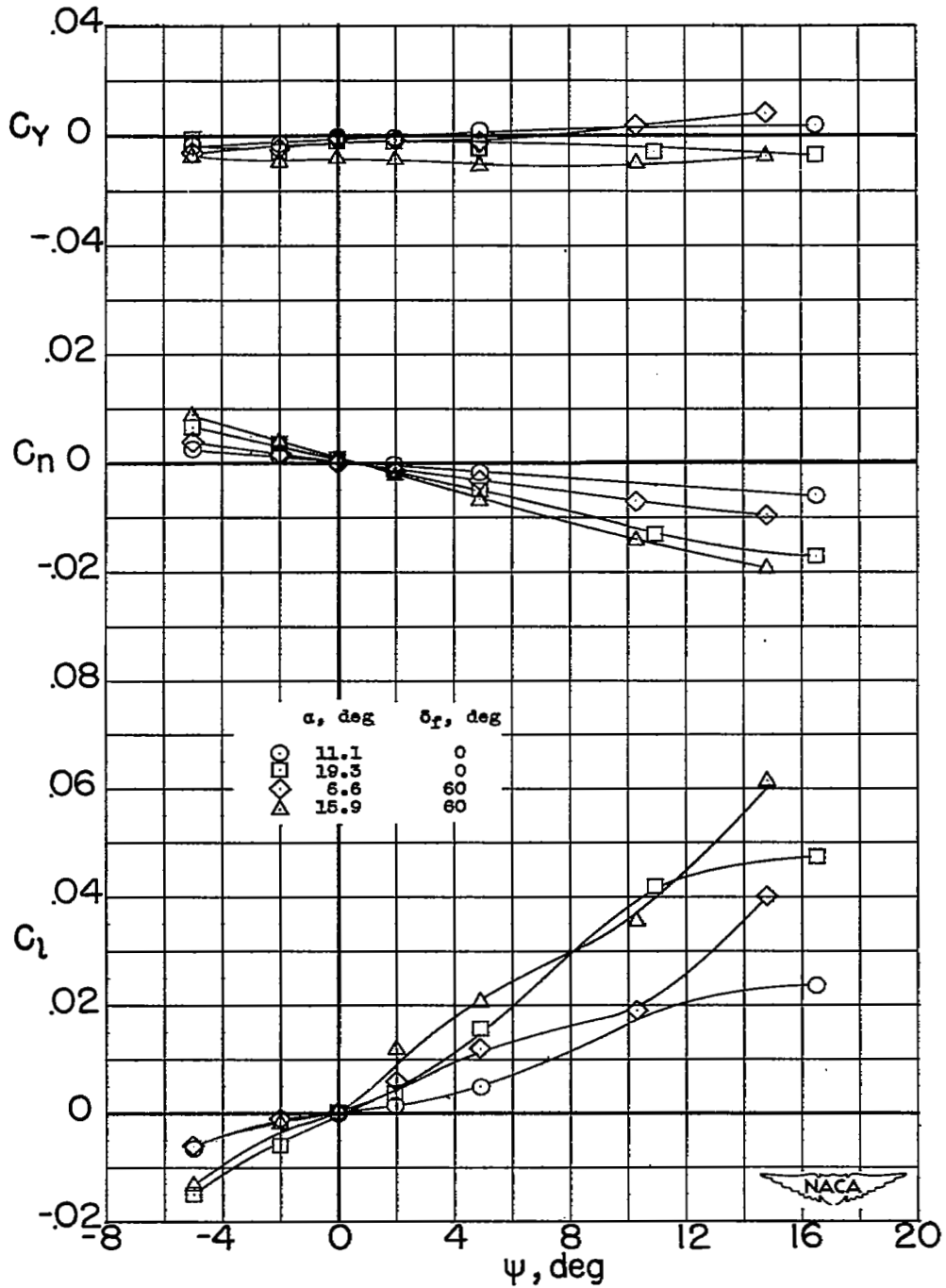
(b) Variation of  $C_L$ ,  $C_X$ , and  $C_m$  with  $\psi$ .

Figure 7.- Concluded.



(a) Variation of  $C_L$ ,  $C_M$ , and  $C_Y$  with  $\psi$ .

Figure 8.- Aerodynamic characteristics in yaw of wing with full-span leading-edge flap installed.  $R \approx 3.5 \times 10^6$ .

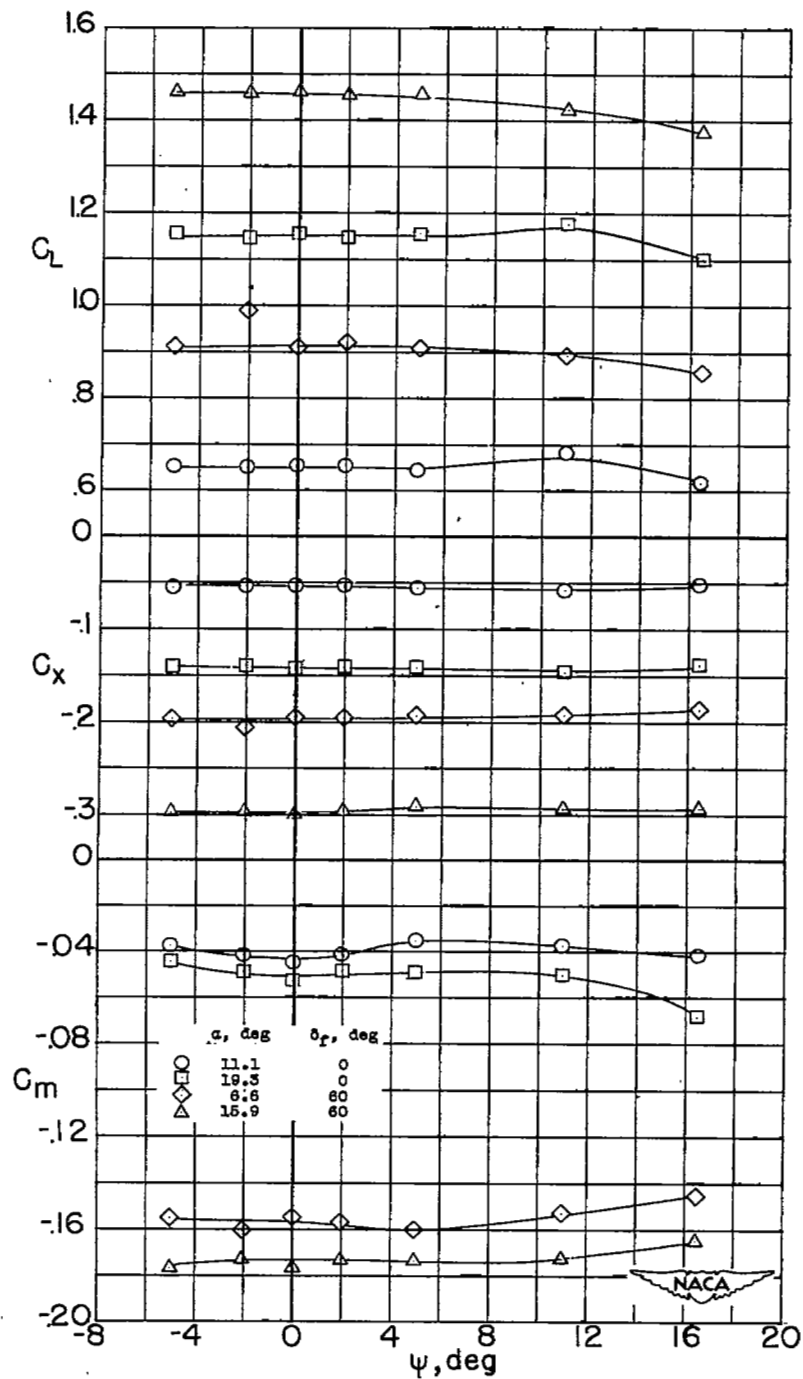
(b) Variation of  $C_L$ ,  $C_X$ , and  $C_m$  with  $\psi$ .

Figure 8.- Concluded.

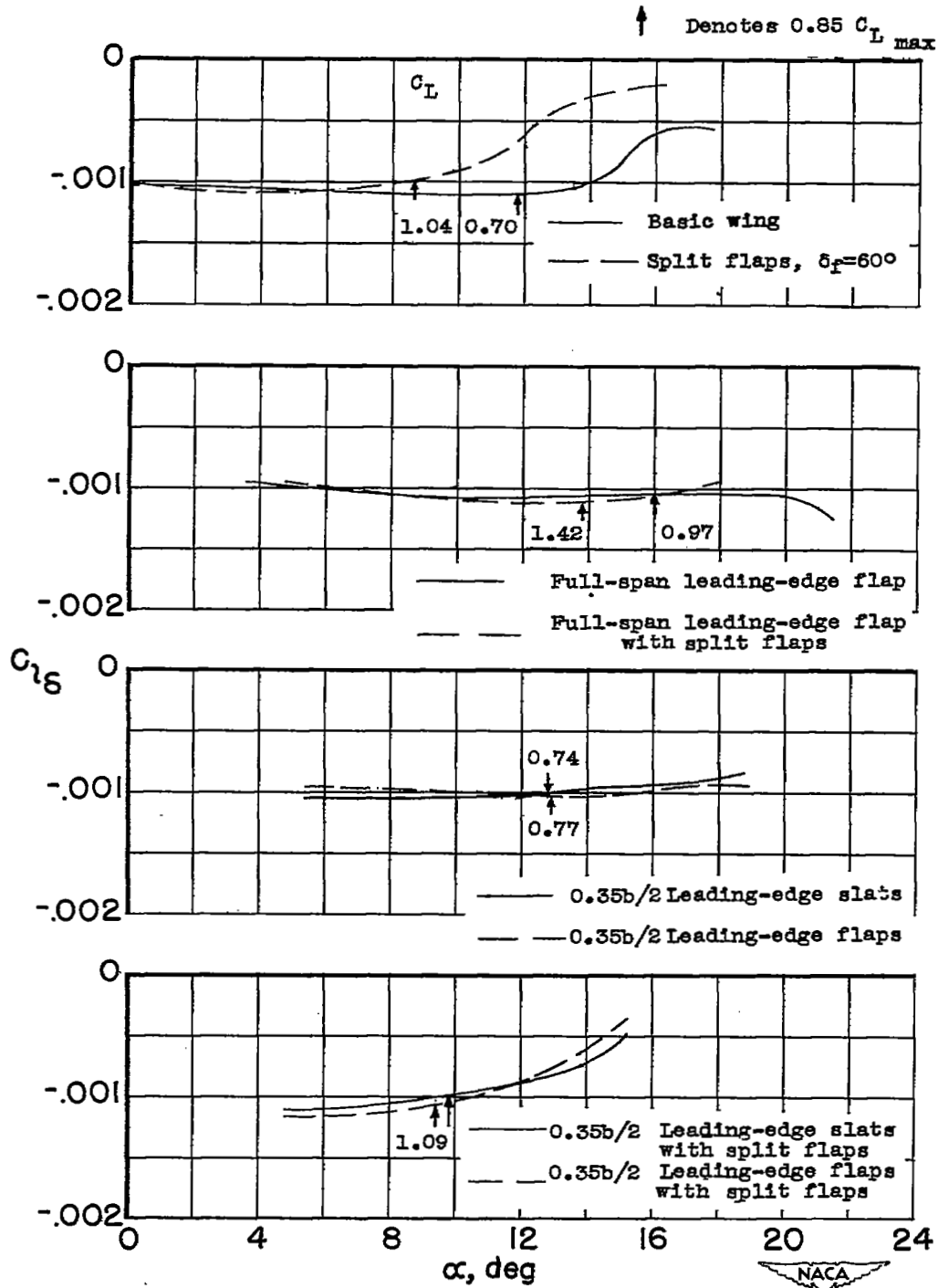
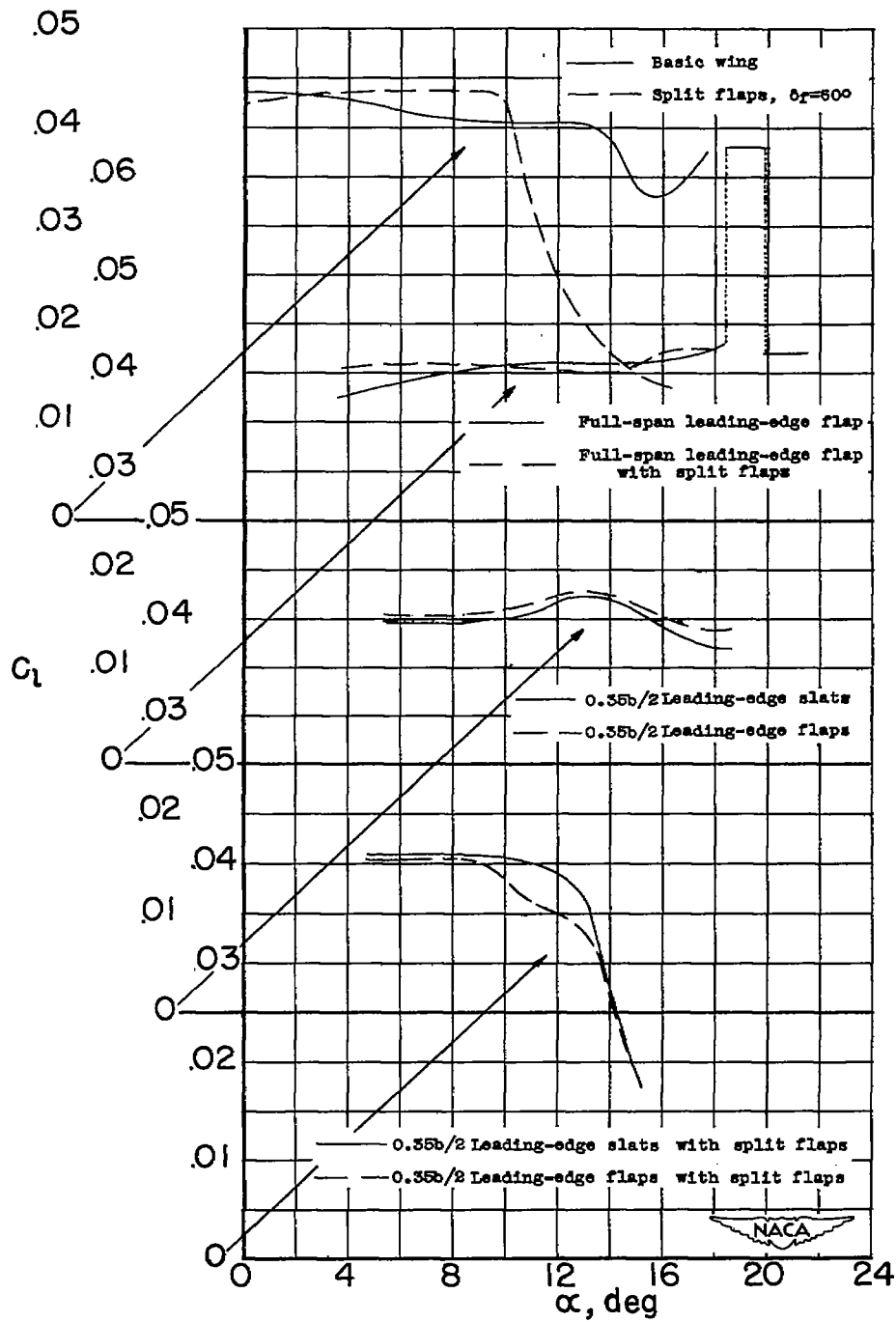
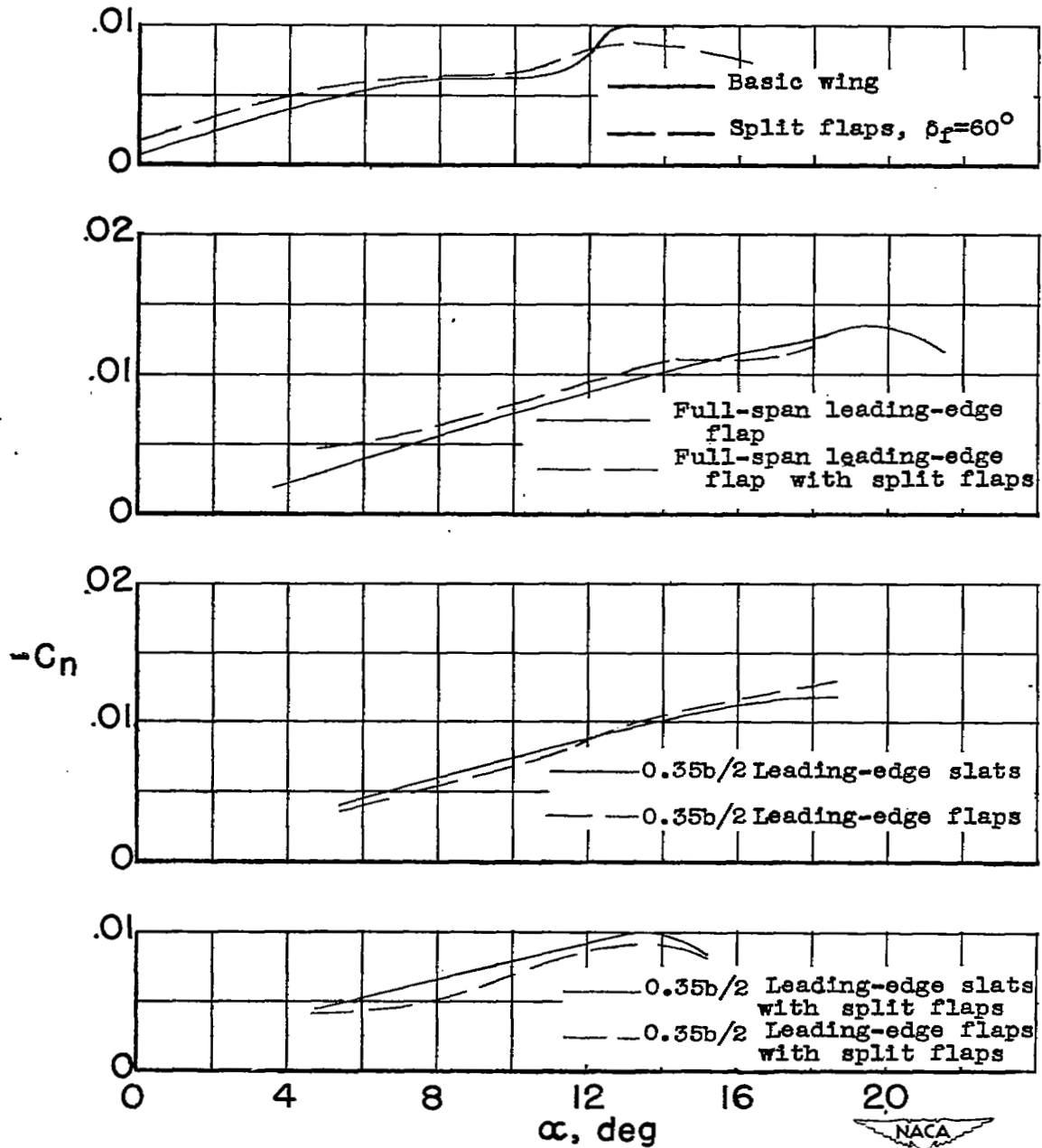


Figure 9.- Summary curves showing the effects of high-lift devices on the aileron-effectiveness parameter  $C_L\delta$ .  $R \approx 3.5 \times 10^6$ .



(a) Rolling-moment coefficients.

Figure 10.- Rolling- and yawing-moment characteristics for a total aileron deflection of  $48^\circ$  in positive roll.



(b) Yawing-moment coefficients.

Figure 10.- Concluded.

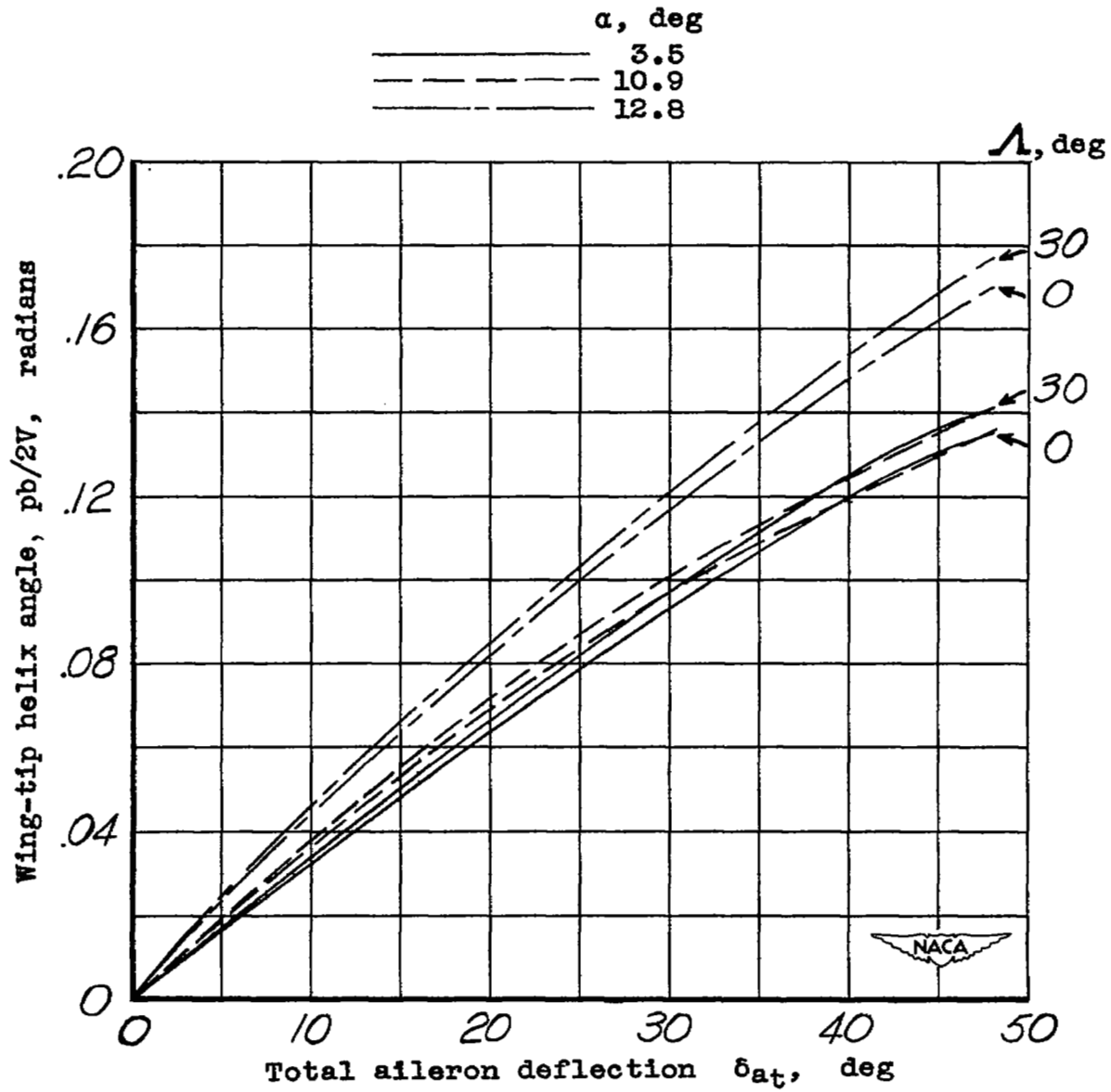
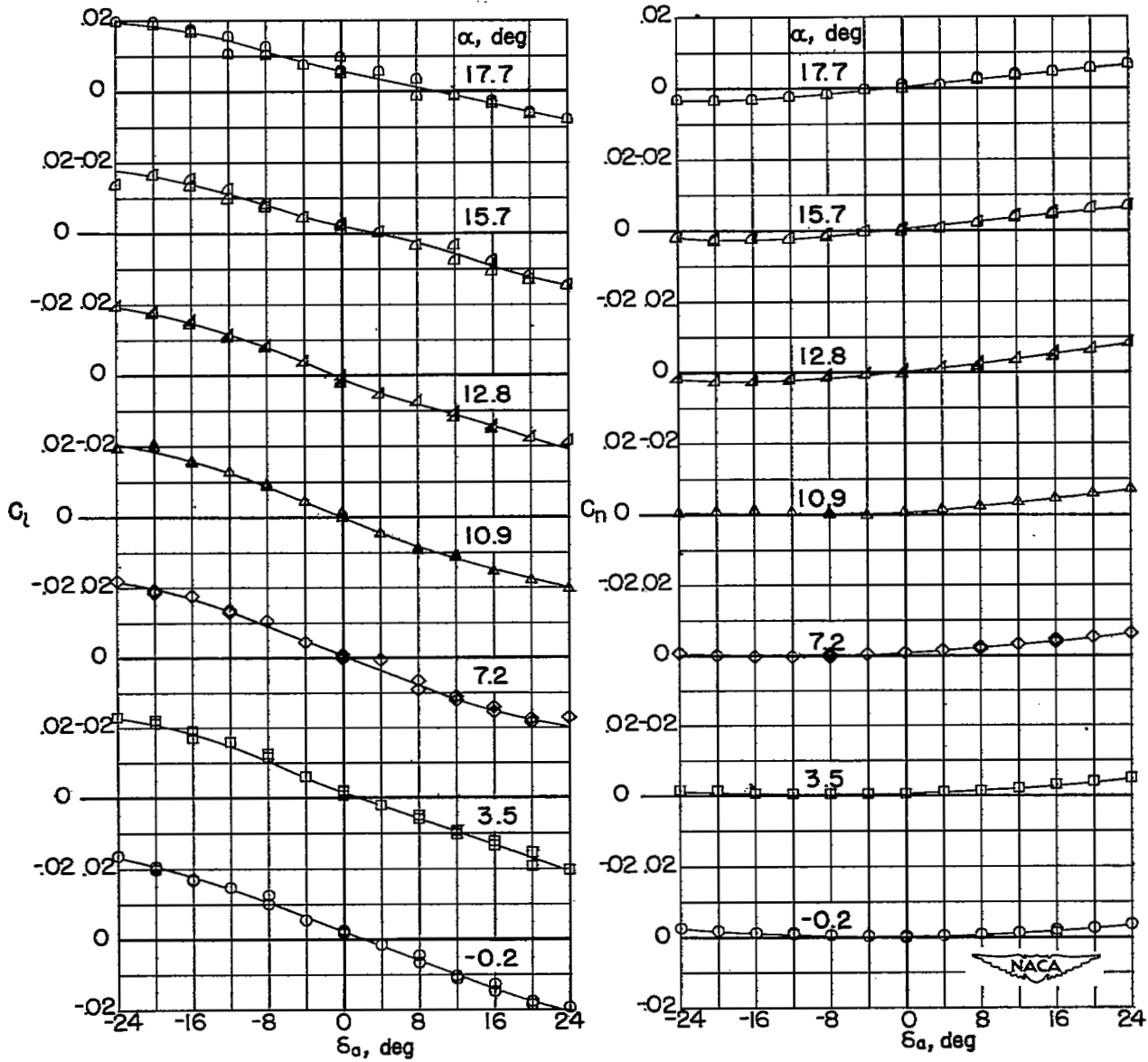


Figure 11.- Variation of estimated wing-tip helix angle  $pb/2V$  with total aileron deflection for the basic wing.



(a)  $C_l$  and  $C_n$  against  $\delta_a$ .

Figure 12.- Aileron characteristics of basic wing.  $R \approx 3.5 \times 10^6$ .

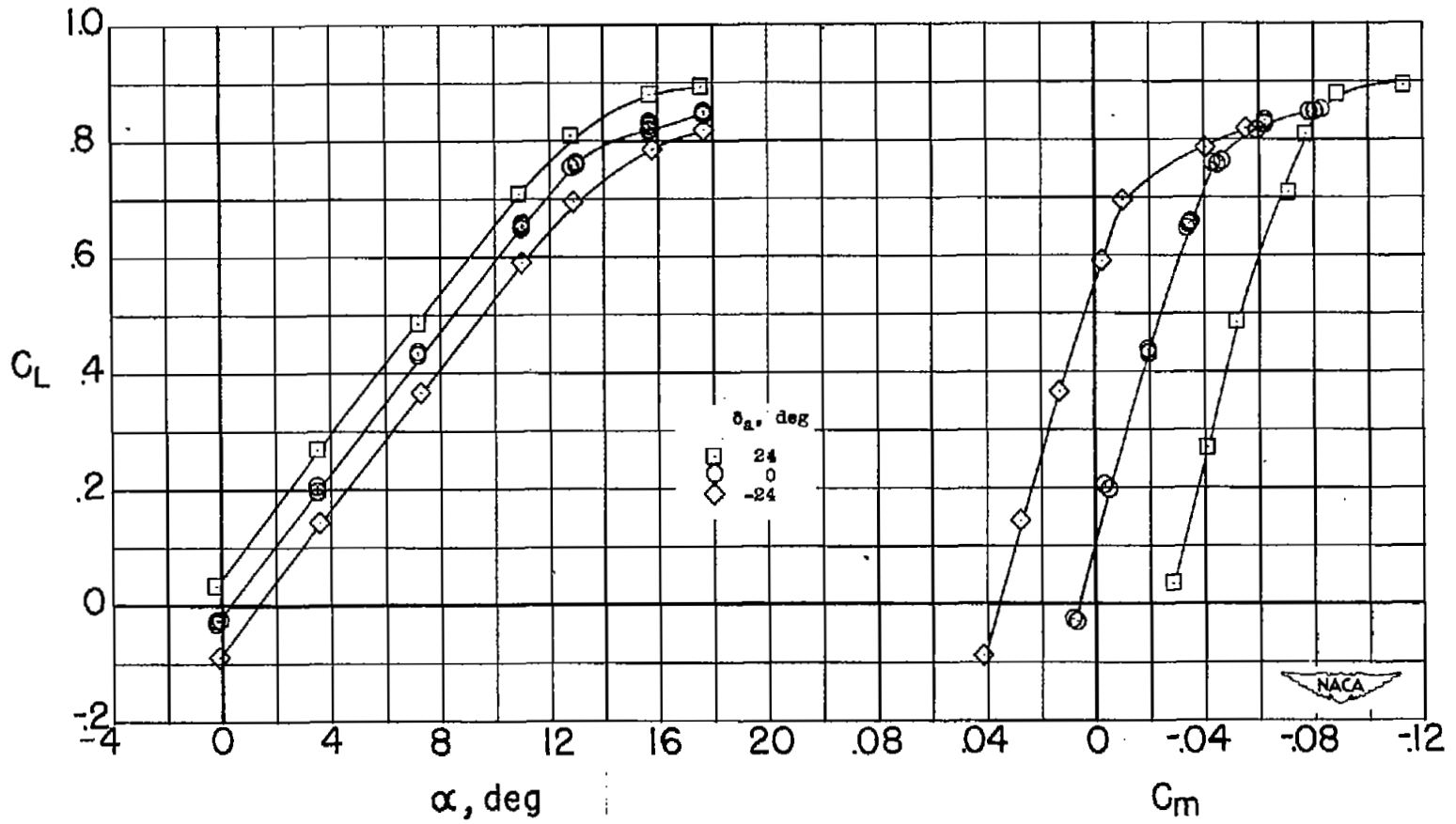
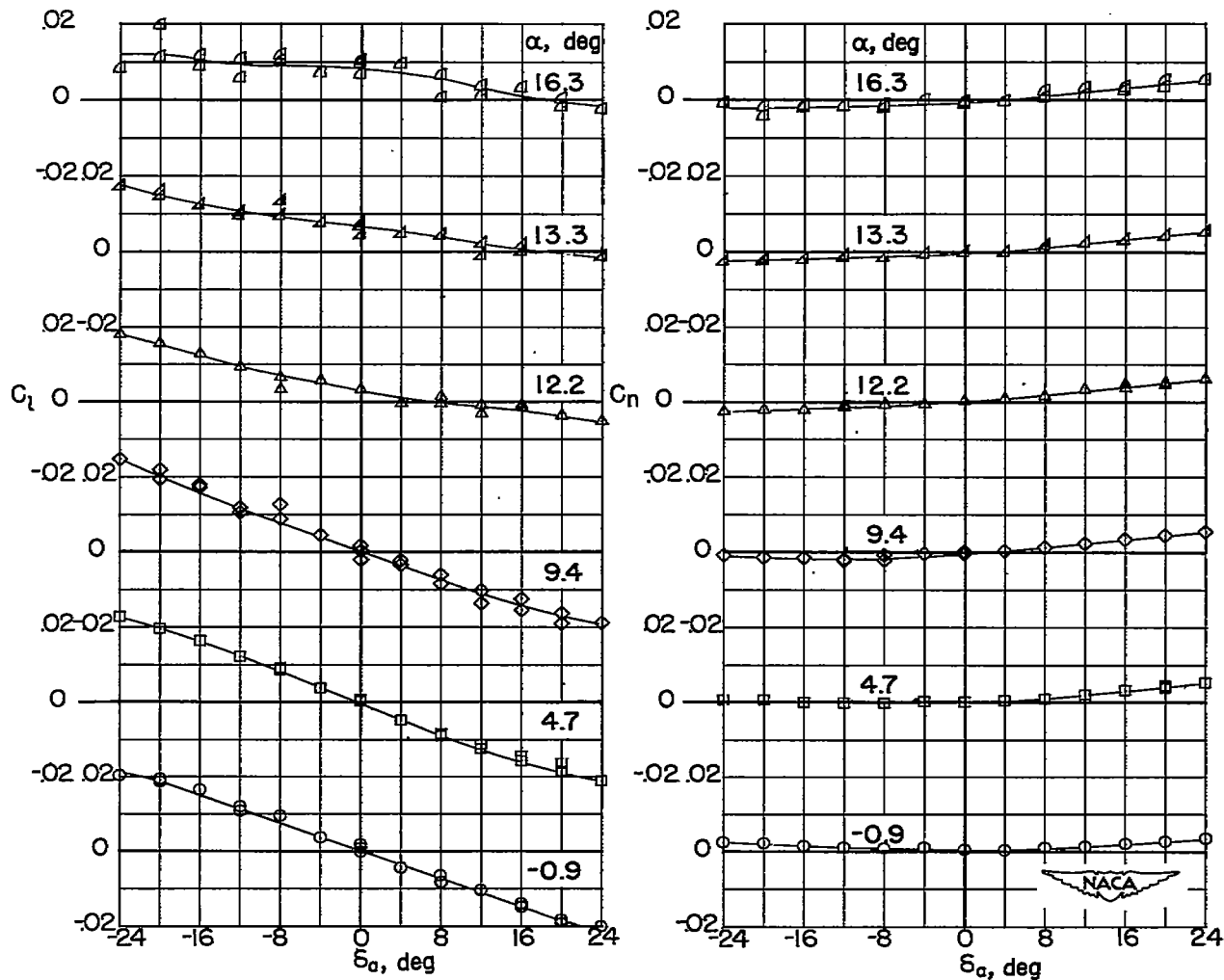
(b)  $C_L$  against  $\alpha$  and  $C_m$ .

Figure 12.- Concluded.



(a)  $C_l$  and  $C_n$  against  $\delta_a$ .

Figure 13.- Aileron characteristics of wing with split flaps installed.

$R \approx 3.5 \times 10^6$ .

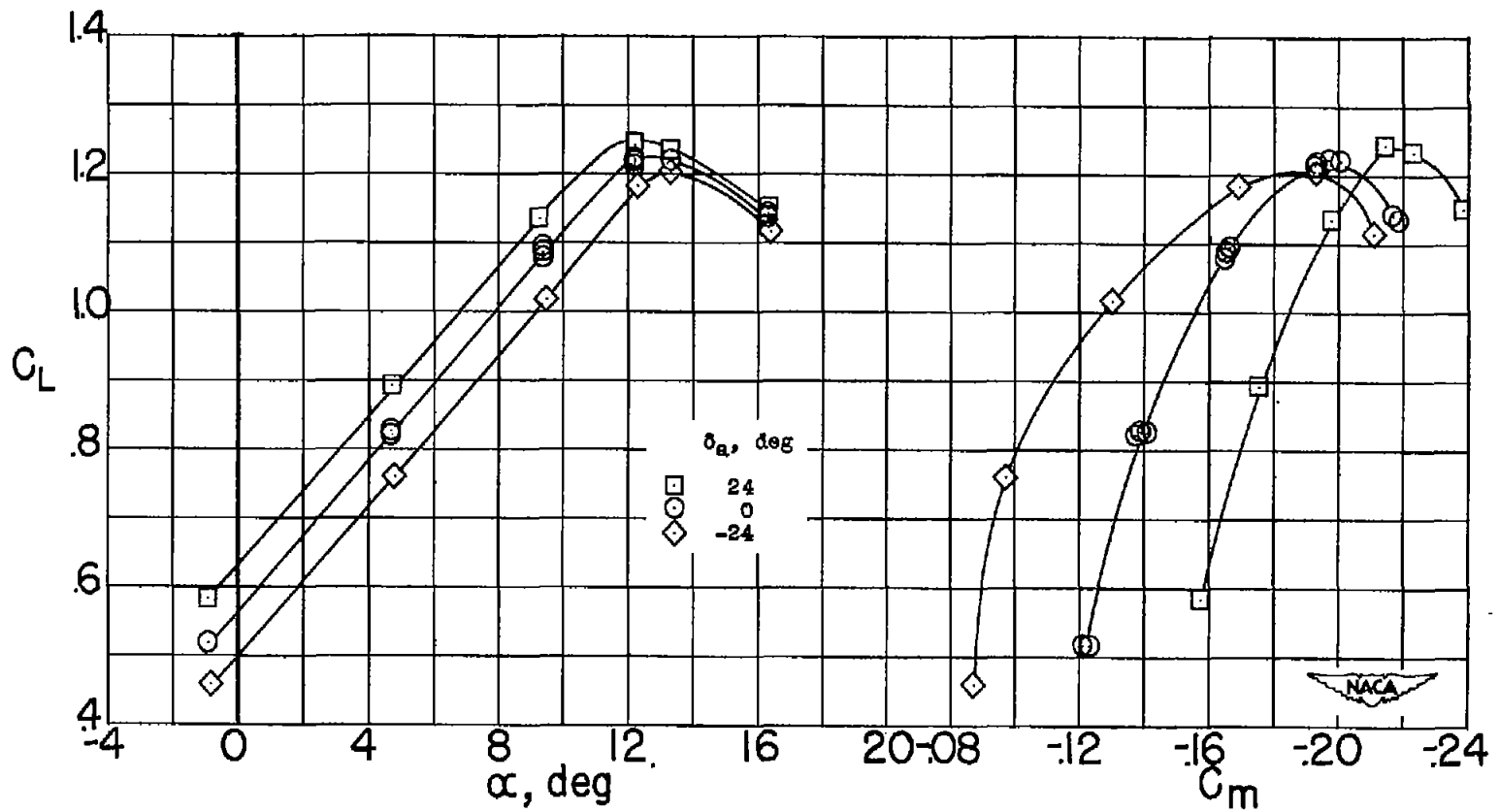
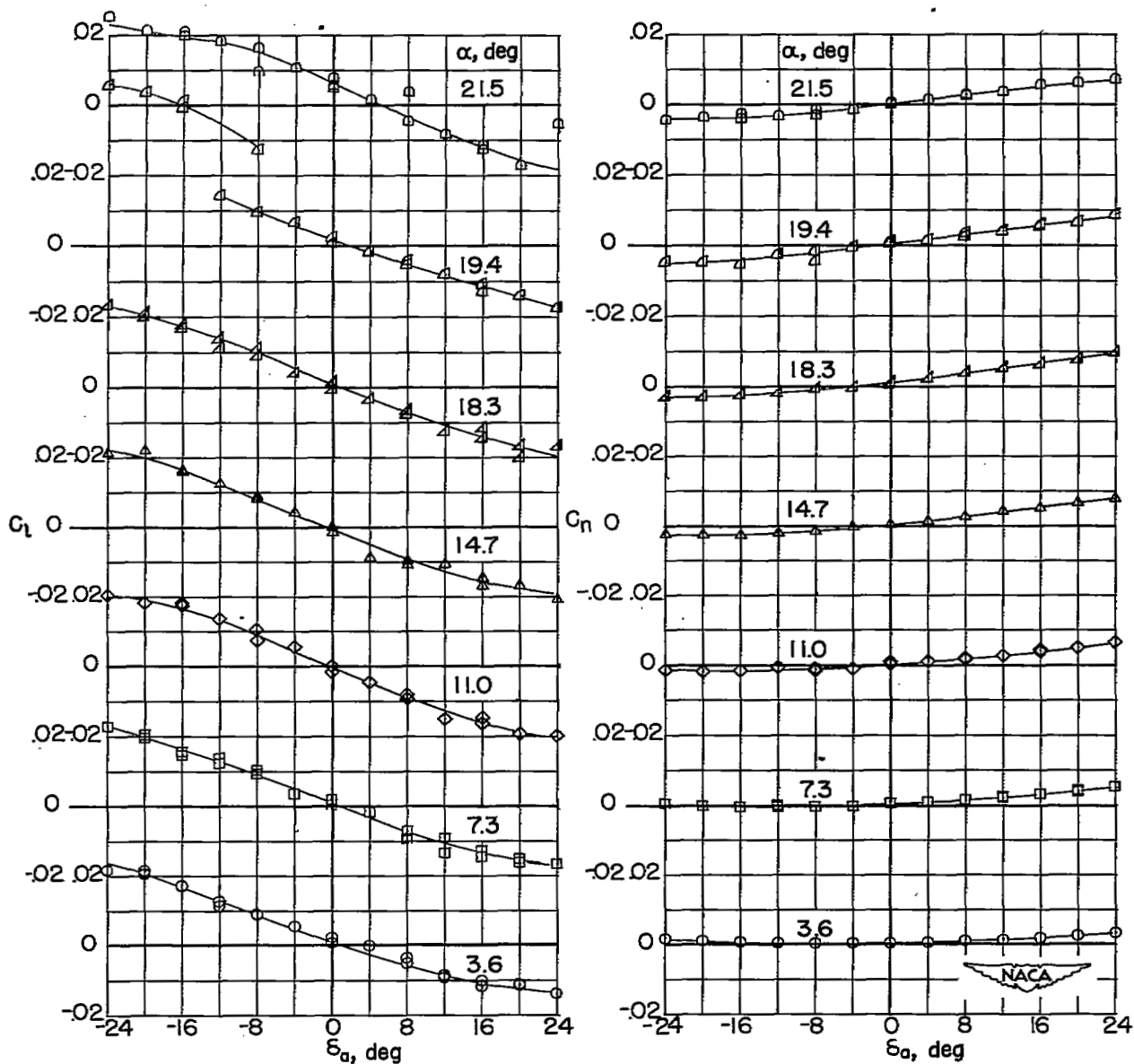
(b)  $C_L$  against  $\alpha$  and  $C_m$ .

Figure 13.- Concluded.



(a)  $C_l$  and  $C_n$  against  $\delta_a$ .

Figure 14.- Aileron characteristics of wing with full-span leading-edge flap installed.  $R \approx 3.5 \times 10^6$ .

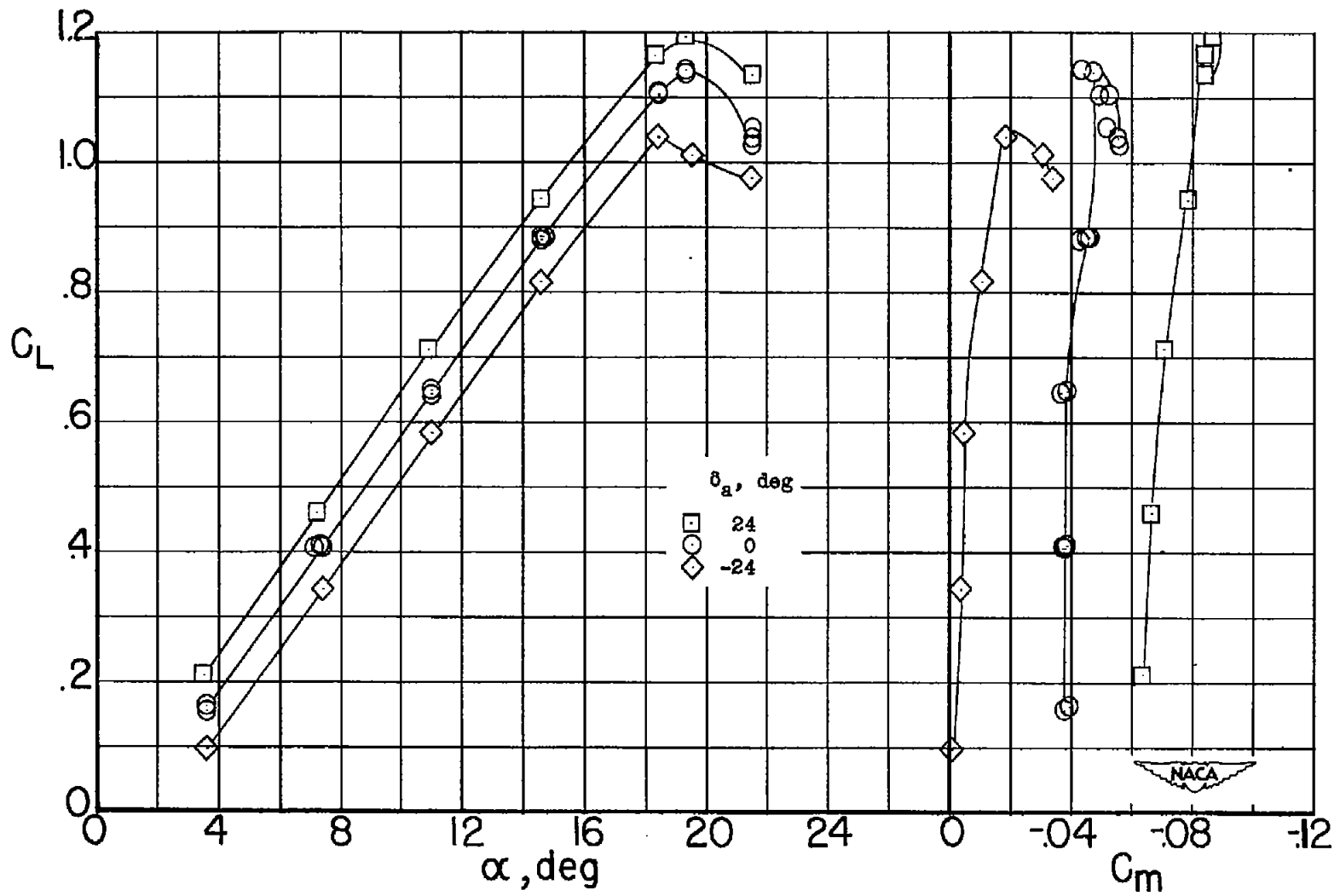
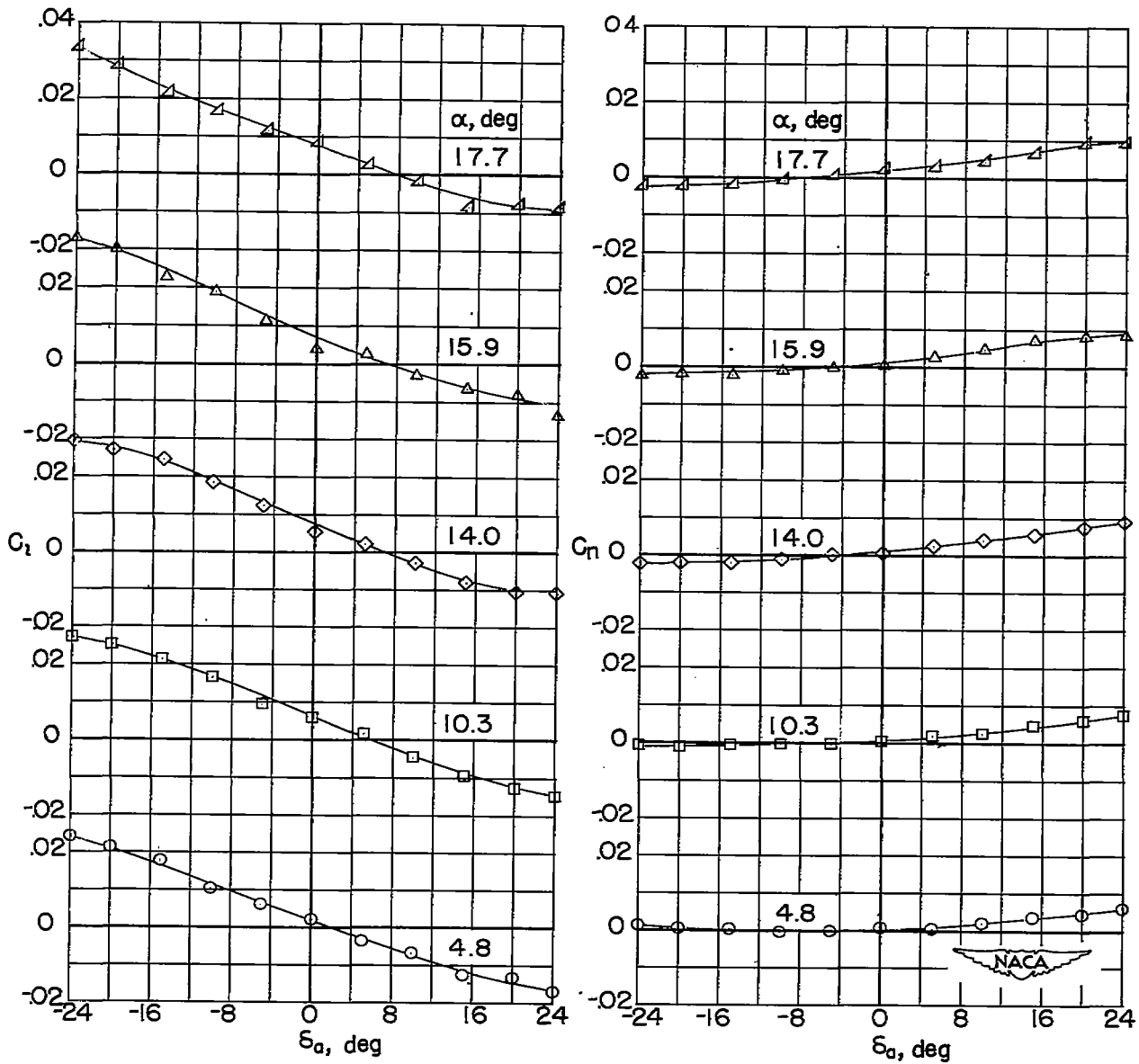
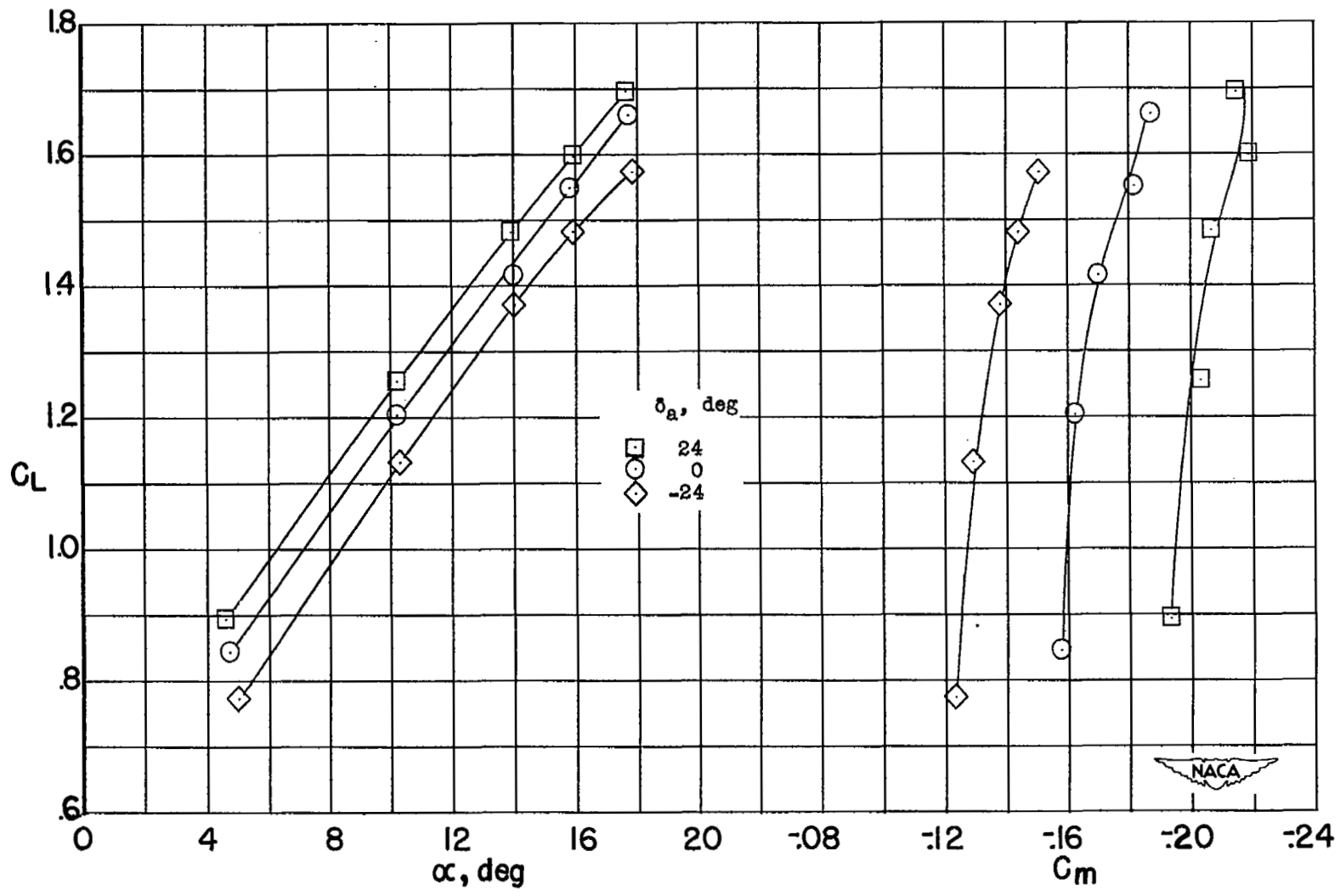
(b)  $C_L$  against  $\alpha$  and  $C_m$ .

Figure 14.- Concluded.



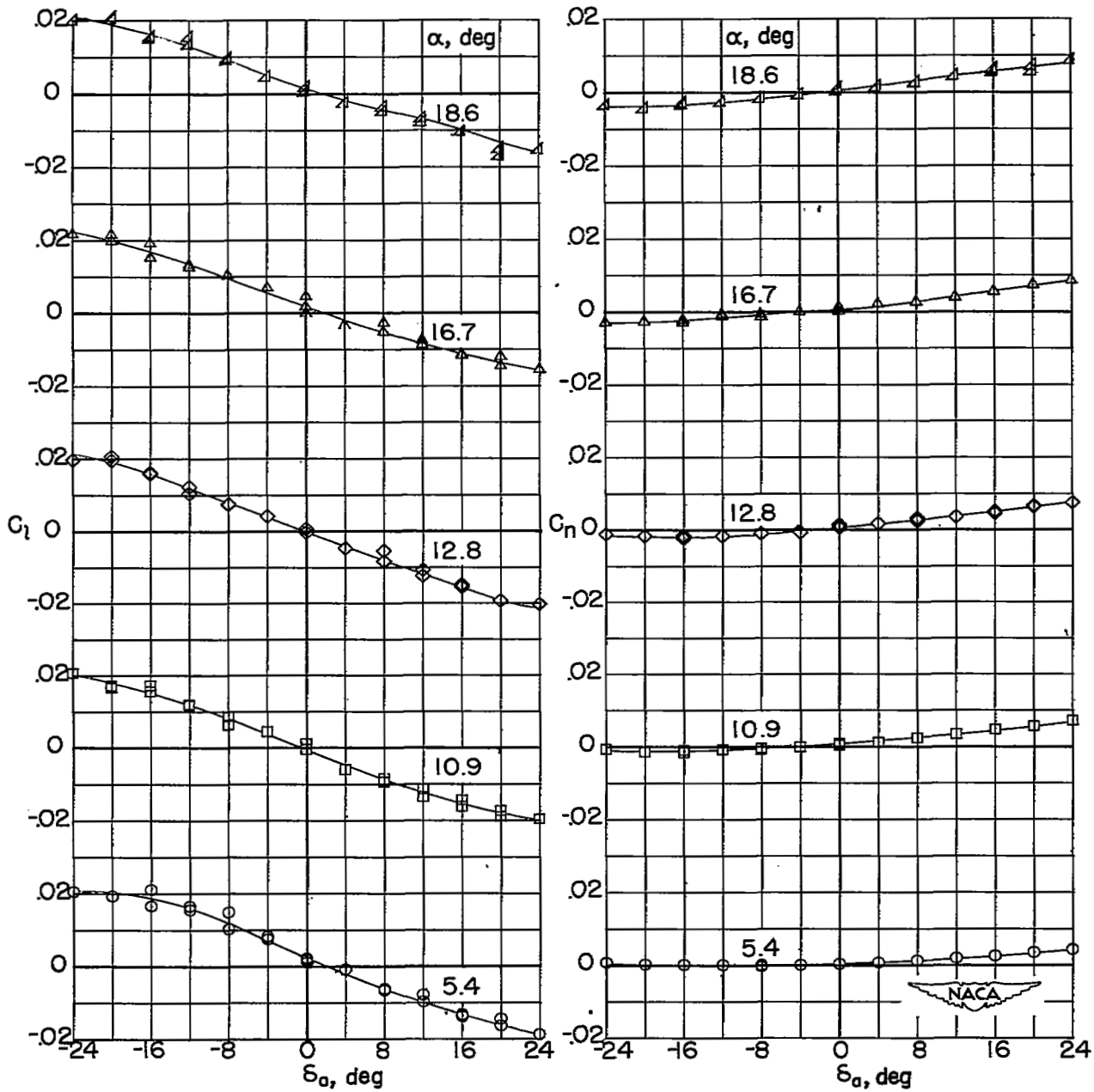
(a)  $C_l$  and  $C_n$  against  $\delta_a$ .

Figure 15.- Aileron characteristics of wing with full-span leading-edge flap and split flaps installed.  $R \approx 3.5 \times 10^6$ .



(b)  $C_L$  against  $\alpha$  and  $C_m$ .

Figure 15.- Concluded.



(a)  $C_l$  and  $C_n$  against  $\delta_a$ .

Figure 16.- Aileron characteristics of wing with  $0.35b/2$  leading-edge slats installed.  $R \approx 3.5 \times 10^6$ .

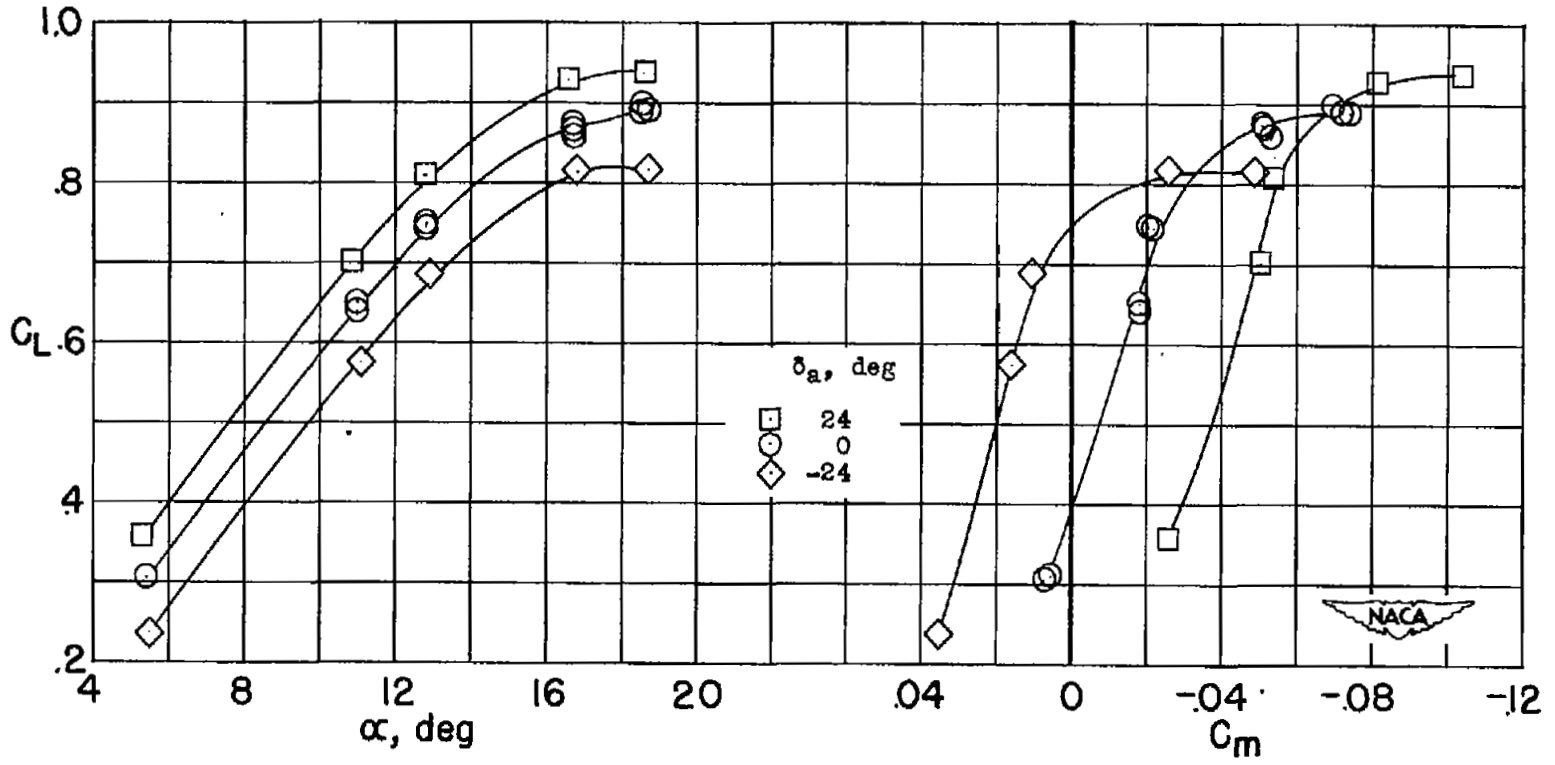
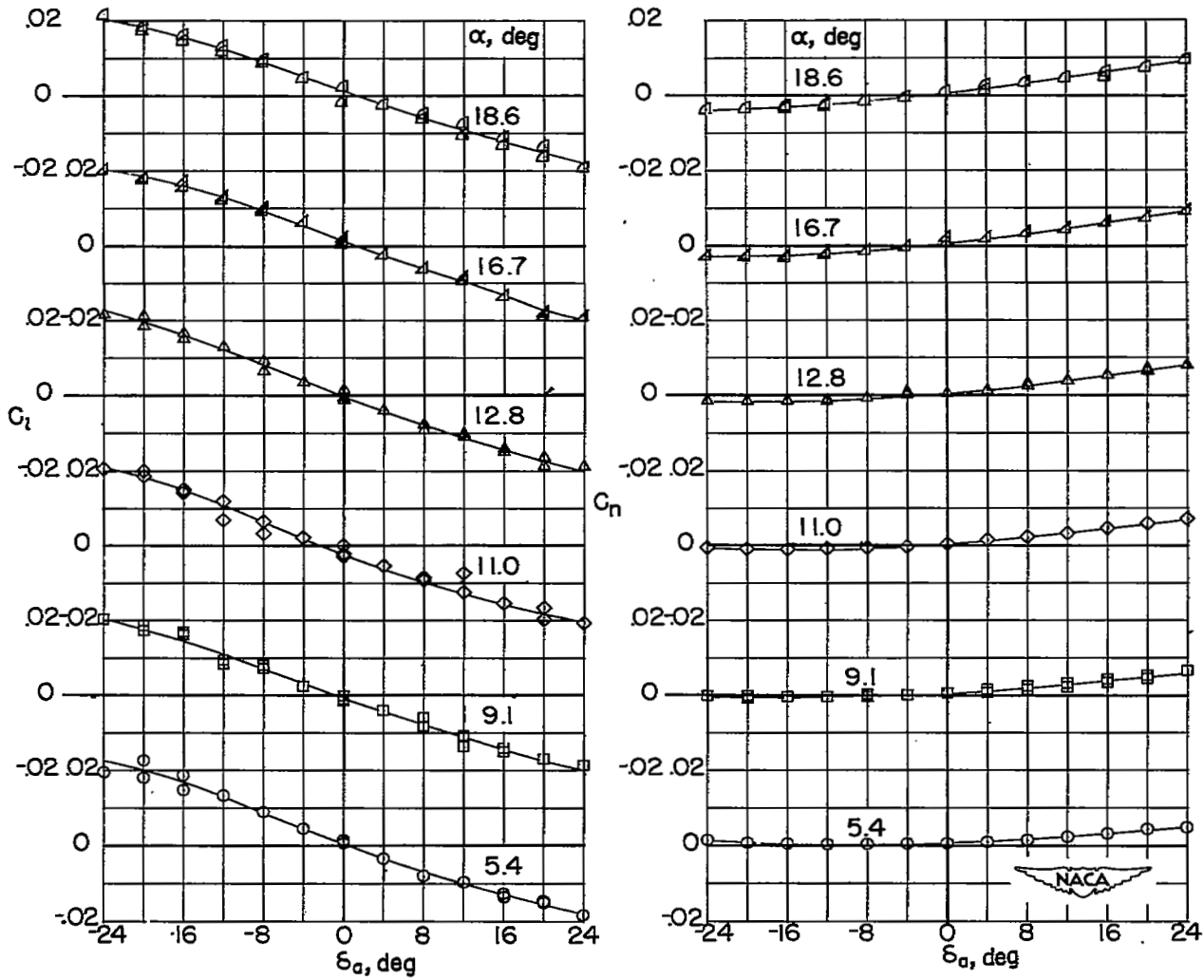
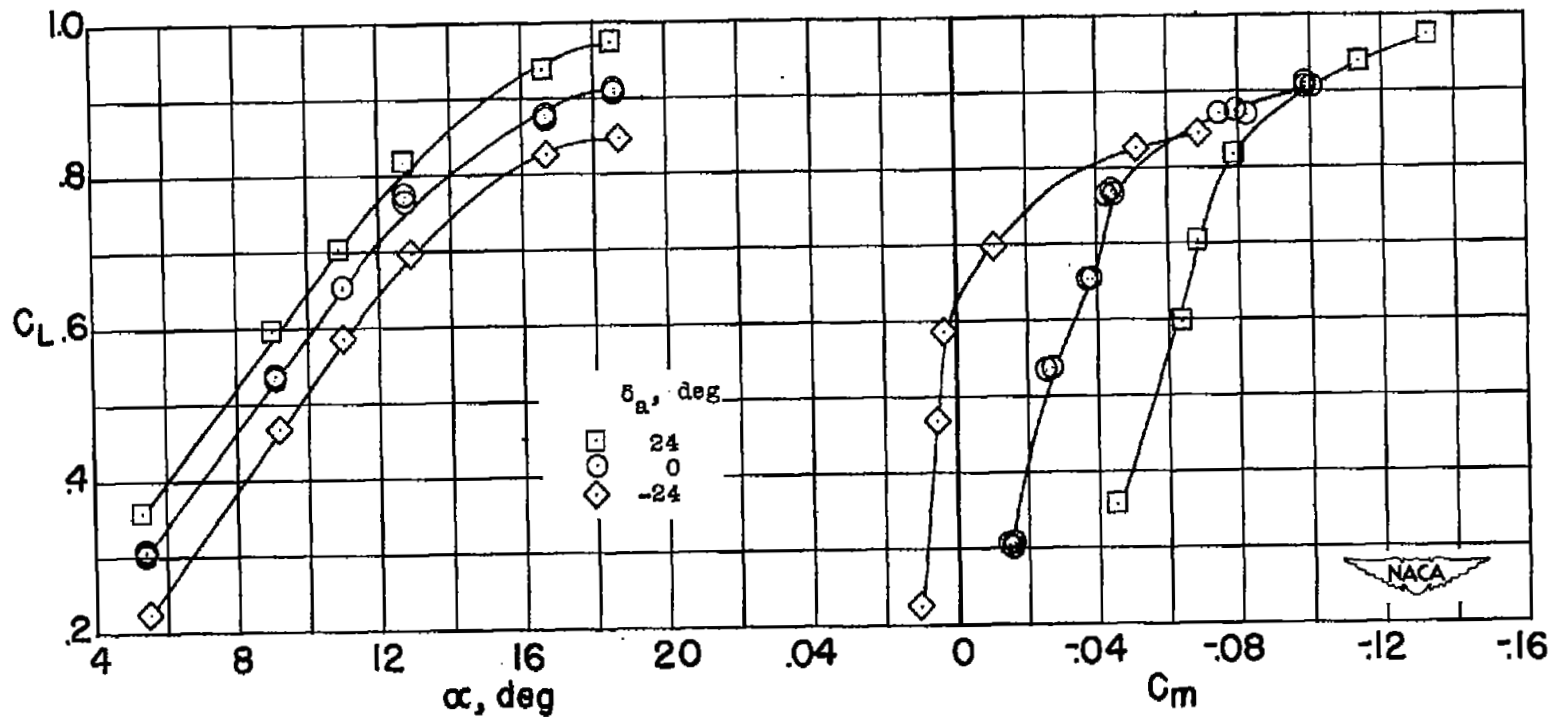
(b)  $C_L$  against  $\alpha$  and  $C_m$ .

Figure 16.- Concluded.



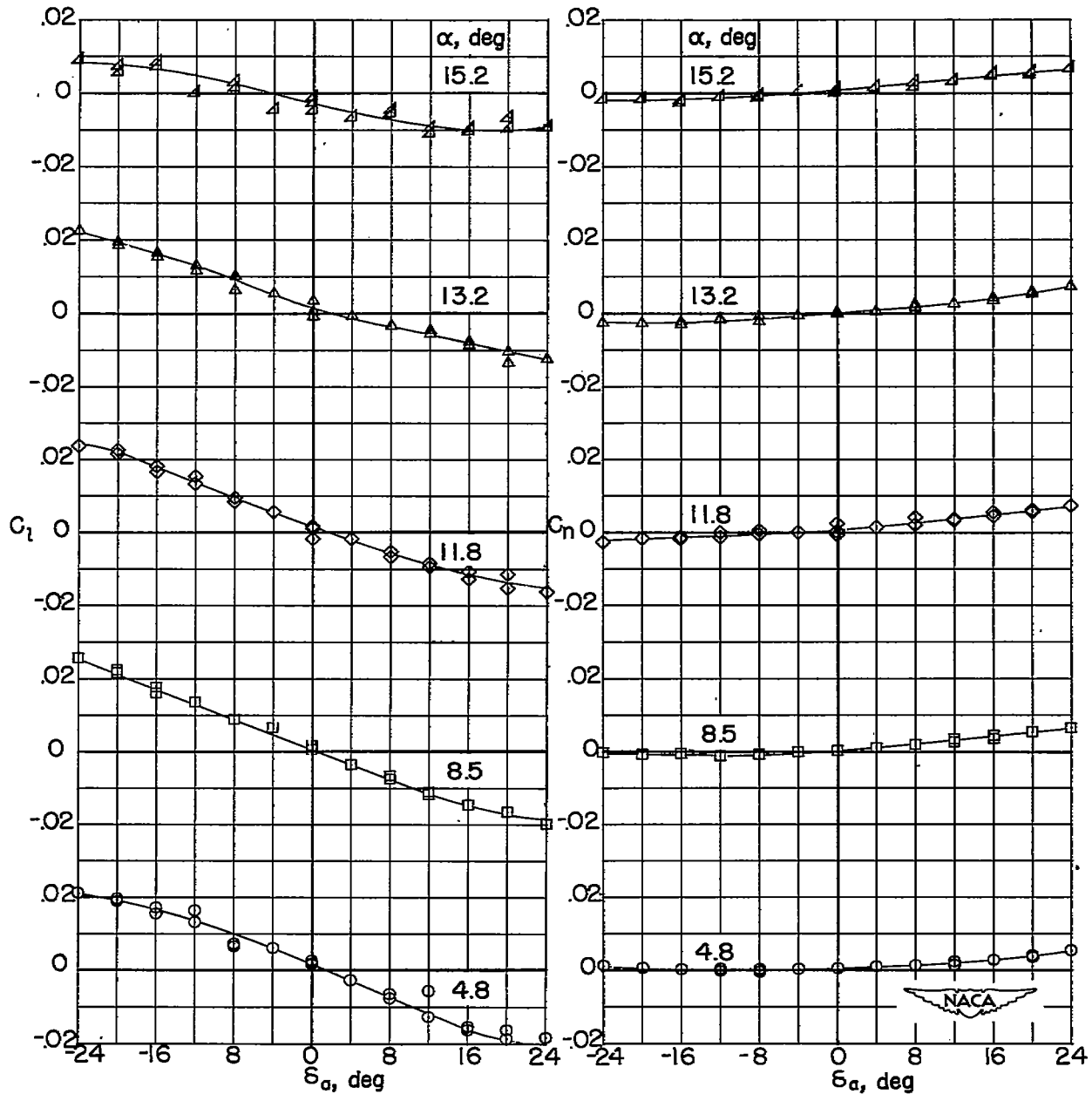
(a)  $C_l$  and  $C_n$  against  $\delta_a$ .

Figure 17.- Aileron characteristics of wing with  $0.35b/2$  leading-edge flaps installed.  $R \approx 3.5 \times 10^6$ .



(b)  $C_L$  against  $\alpha$  and  $C_m$ .

Figure 17.- Concluded.



(a)  $C_l$  and  $C_n$  against  $\delta_a$ .

Figure 18.- Aileron characteristics of wing with  $0.35b/2$  leading-edge slats and split flaps installed.  $R \approx 3.5 \times 10^6$ .

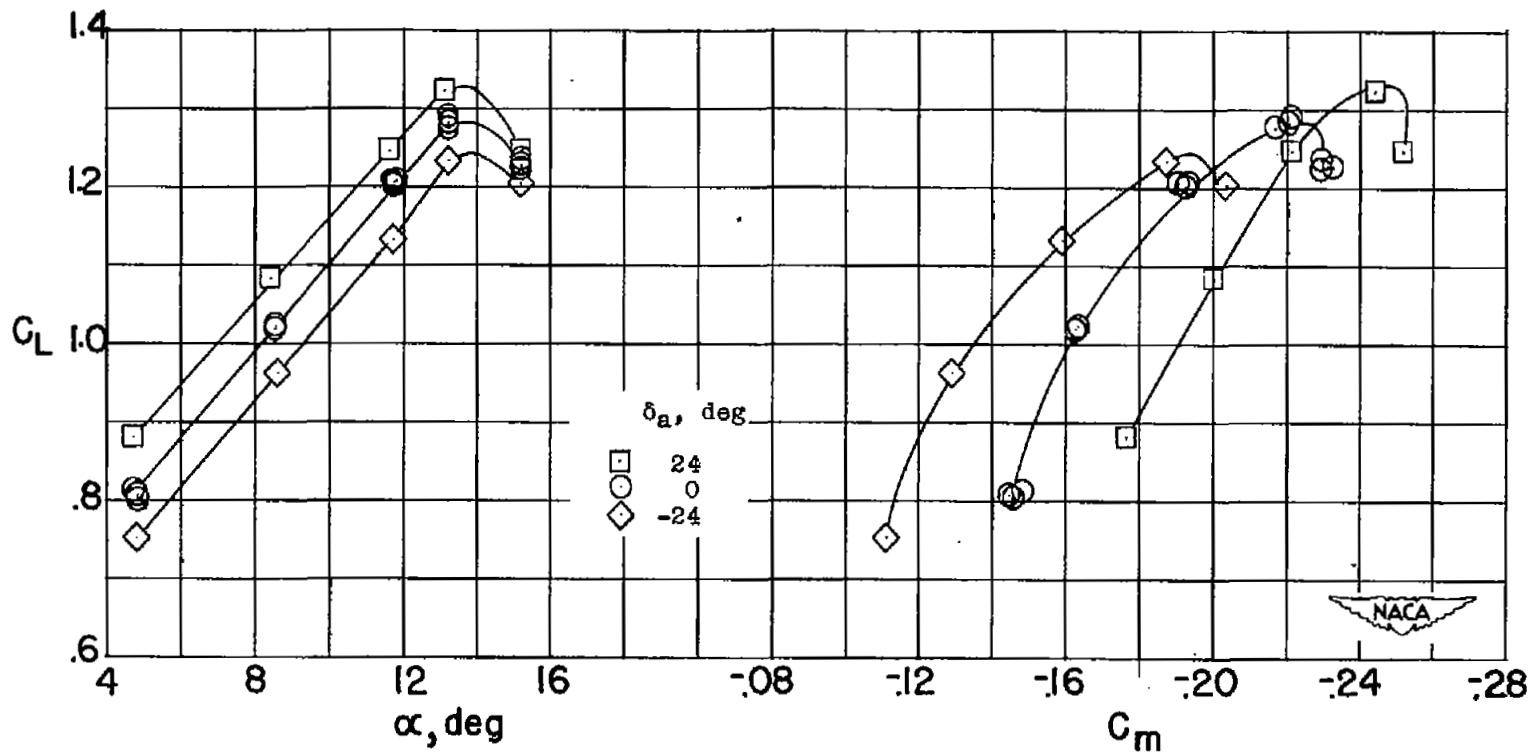
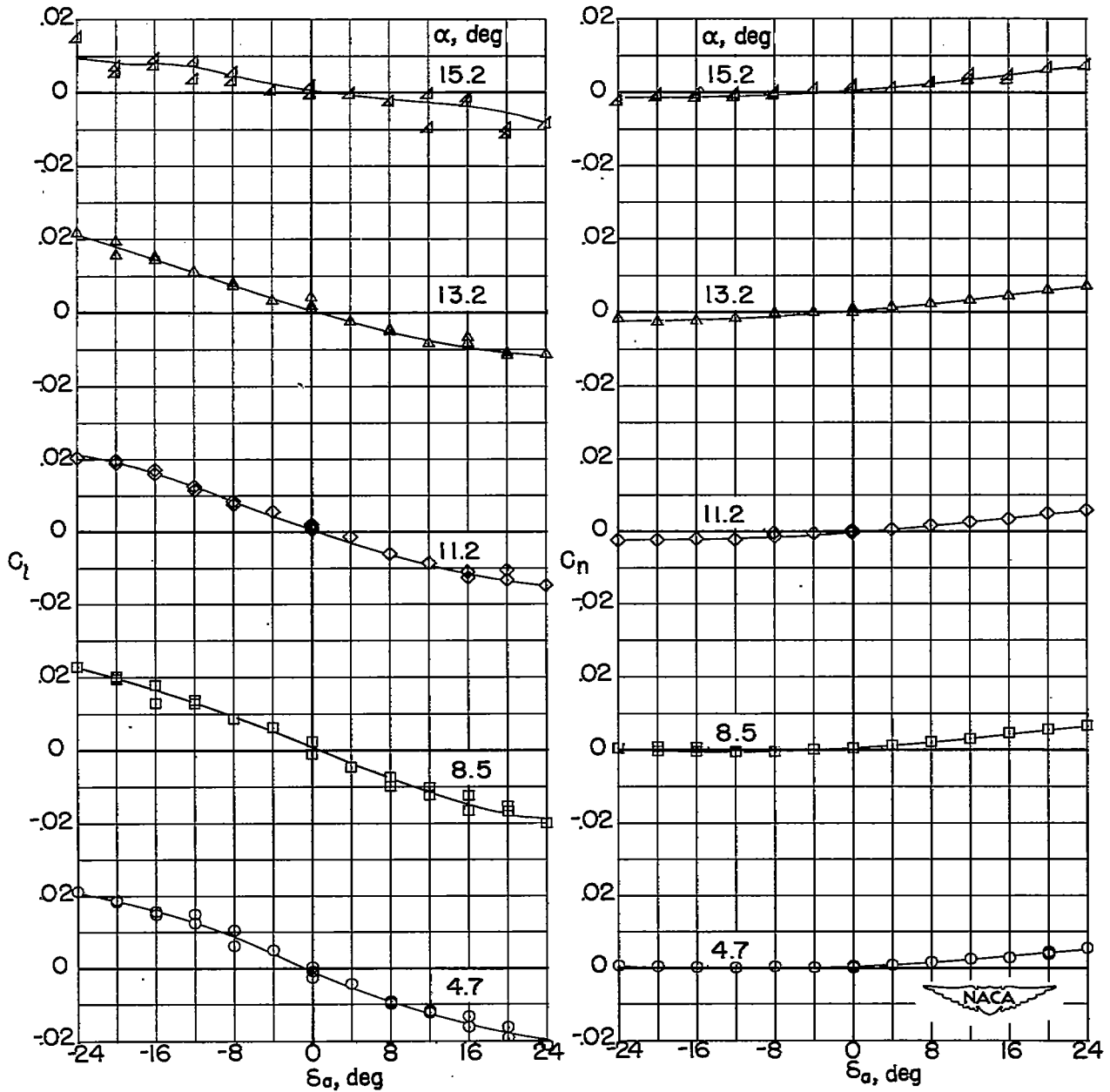
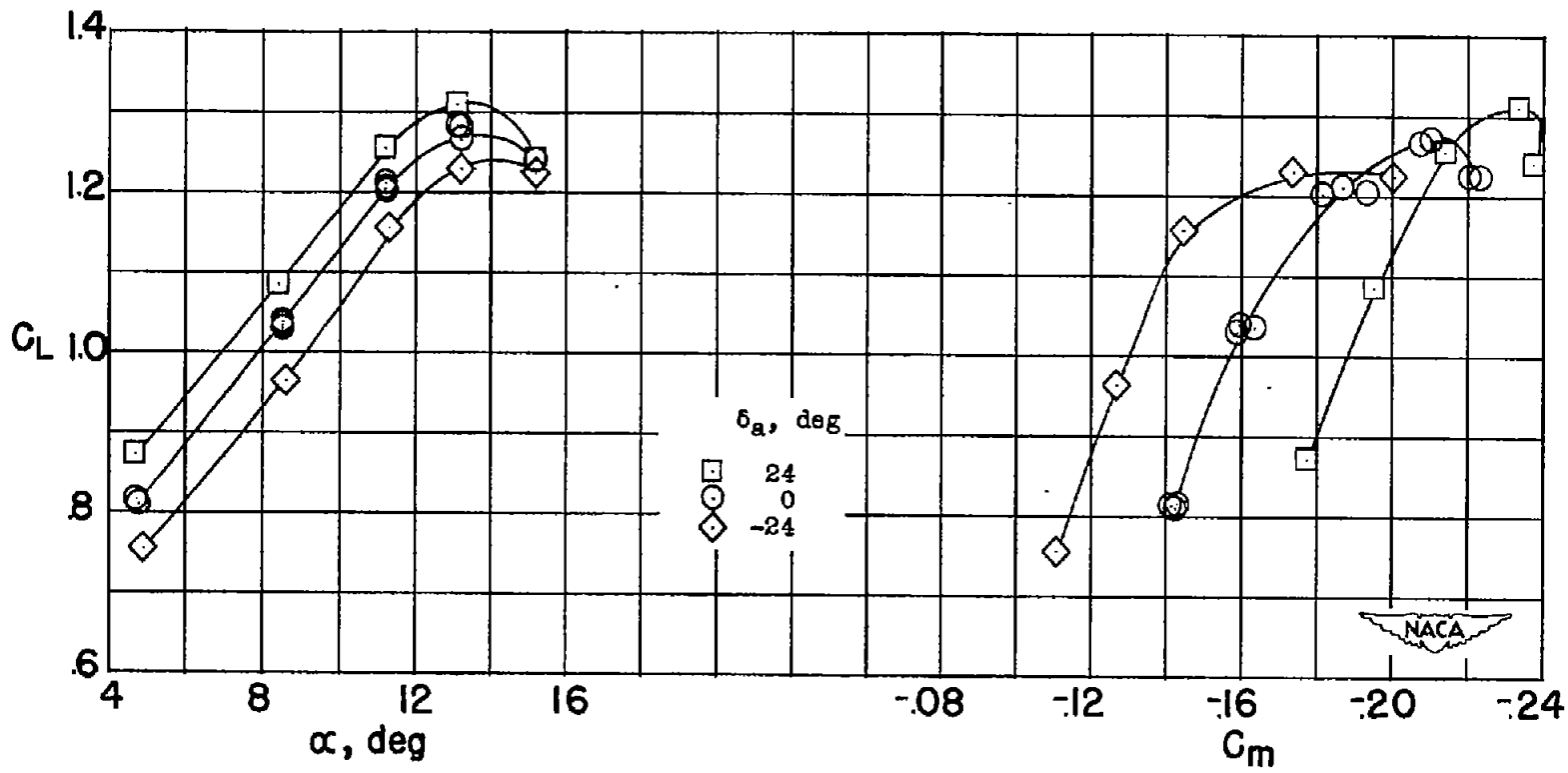
(b)  $C_L$  against  $\alpha$  and  $C_m$ .

Figure 18.- Concluded.



(a)  $C_l$  and  $C_n$  against  $\delta_a$ .

Figure 19.- Aileron characteristics of wing with  $0.35b/2$  leading-edge flaps and split flaps installed.  $R \approx 3.5 \times 10^6$ .



(b)  $C_L$  against  $\alpha$  and  $C_m$ .

Figure 19.- Concluded.